AFM STUDY OF CHARGE TRANSPORT MECHANISMS AT ELECTRICAL CONTACTS IN METAL-MOLECULE-METAL SYSTEMS

by

Chang Min Kim

M.S., Hanyang University 1998

THESIS SUBMITTED IN PARTIAL FULFILLMENT

OF THE REQUIREMENTS FOR THE DEGREE OF

MASTER OF SCIENCE

IN THE

DEPARTMENT OF PHYSICS

FACULTY OF SCIENCE

SIMON FRASER UNIVERSITY

Summer, 2011

APPROVAL

Name:	Chang Min Kim
Degree:	Master of Science
Title of thesis:	AFM Study of Charge Transport Mechanisms at Electrical Contacts in Metal-Molecule-Metal Systems
Examining Committee:	Steve Dodge (Chair)

_____

John Bechhoefer

_____

George Kirczenow

_____

Karen Kavanagh

_____

Eldon Emberly

Date Approved: 7th. July, 2011

Partial Copyright Licence

Abstract

We investigated charge transport mechanisms at the interface between 1,8 octanedithiol (ODT) and gold and platinum electrodes. We used a voltage-biased, conductive-probe atomic force microscope tip (CP-AFM) to repeatedly break the bond between a molecule and an electrode and compiled statistics of the measured conductances for gold (Au) and platinum (Pt) electrodes. We examined the conductances of the Au-ODT-Au, Au-ODT-Pt, and Pt-ODT-Pt systems and observed at least two kinds of conductance mechanisms. The conductances were ordered, Pt-ODT-Pt > Pt-ODT-Au > Au-ODT-Au, which is consistent with a charge-transport mechanism through the junction that is proportional to the number of electron channels and depends on the molecular distance between the ligand group at the end of the ODT and the electrode. We investigated the electronic properties of the thiol-metal junction by measuring conductances as a function of bias voltage. We observed a nonlinear junction response that we attribute to a resonance among interface states in the junction. The junction stability was investigated by measuring the conductance step-length, which we correlated with the chemical binding energy.

Tribute to God, Soo Kyung and My parents

Acknowledgments

I am very happy to finish my thesis. This thesis could not be finished without help and support from many people. First of all, I would like to thank Professor John Bechhoefer, my senior supervisor. He spent so much time correcting and recommending on my thesis to be a legible one. I really appreciate his passion and attitude toward great accuracy in the work. I also thank Professor George Kirczenow and Karen Kavenagh, my supervisors for useful discussions. They allowed their time and shared their precious knowledge. I really thank professor Patricia Mooney for let me use her AFM and closed liquid cell.

Many thanks for the help on programming and discussions to Michel, Scott, and Yong-gun - my labmates. They encouraged and listened me when I asked their opinions and I was distressed. I also thank to professor Hogan Yu, and Lily and other group members of his group. They let me use their resource in material and useful discussion. I would appreciate to Mr. Chris Balicki at 4DLABS for making Pt samples.

Most of all, I appreciate with love to Soo Kyung, my wife. Her support and prayer was the source of power that I was able to come through here. All glory to God.

Contents

List of Tables

List of Figures

Chapter 1

Introduction

Our life today has changed so much compared with a century ago. Electronic devices such as LCD televisions, MP3 players, and computers—all these would have seemed miraculous to someone a hundred years ago. And semiconductor electronics has played the major role in making these miracles possible [1]. In a 1959 lecture at the American Physical Society, Richard Feynman said,

> "*I don't know how to do this on a small scale in a practical way, but I do know that computing machines are very large; they fill rooms. Why can't we make them very small, make them of little wires, little elements – and by little, I mean little. For instance, the wires should be 10 or 100 atoms in diameter, and the circuits should be a few thousand angstroms across...there is plenty of room to make them smaller. There is nothing that I can see in the physical laws that says the computer elements cannot be made enormously smaller than they are now. In fact, there may be certain advantages.*" [2]

As Feynman predicted, the miniaturization of solid-state electronics has led to emerging devices. However, the current "top-down" approach based on semiconductor technologies must, at some point, reach its limit as sizes approach molecular dimensions [1, 3]. Thus, the next breakthrough may start from technology that can manipulate nanometer-scale phenomena.

The idea that molecules can transport charges through them has spawned a new field of research called "molecular electronics," since Aviram and Ratner proposed that a single

molecule could act as an electronic component [4, 1]. The wire-shaped organic molecules that can transport charge through them are called "molecular wires" [5, 6, 7].

To act as an electronic component, these molecular wires should bond to a metal electrode, in a metal-molecule-metal configuration [8, 9]. In many cases, the metal-molecule-metal configuration is formed by a self-assembly process through the linker groups, which are chemical ligands that bind electrodes covalently. The monolayers of the molecules formed by the self-assembly are called "self-assembled monolayers" (SAMs) [10, 11, 12].

Properties of molecular wires have been explored and potential applications are devised based on the development of technologies such as modern lithography [13, 14], scanning tunnelling microscopy (STM, 1981) [15] and atomic force microscopy (AFM, 1986) [16], the synthesis of desired molecules [1], and the application of SAMs [11, 10].

1.1 Self-Assembled Monolayers (SAMs)

Self-assembled monolayers (SAMs) are layers of organic molecular assemblies formed by the spontaneous chemical adsorption of molecules through binding ligands (head group), which can bind covalently to metal atoms of substrate. Self-assembly is also a major process in many biological systems, from single molecules such as DNA to the more complex lipid membranes and, ultimately, to living cells. SAMs provide a simple, convenient, and very flexible way to design properties of metals, semiconductors, and so on. SAMs can make organized, well-packed surfaces more easily than other methods such as molecular beam epitaxy (MBE) and chemical vapor deposition (CVD) [10].

SAMs are formed from a solution containing the molecules by spontaneous chemisorption. Bare surfaces of metals tend to adsorb specific organic materials because the adsorbates lower the free energy of the interface between metal and ambient environment [10]. The molecule forming the monolayer has headgroups that can link specifically with the substrate. Commonly used headgroups include thiols (-SH), carboxyls (-COOH), and amines (-NH_3) [10, 11].

Since the adsorbed ligand is thermodynamically more stable than the bare metal surface, SAMs can be formed on a variety of surfaces, from flat substrates to nanoparticles. Making well-defined SAMs is very simple. For example, in the case of thiol, the most commonly used ligand, one can just immerse a gold substrate in an alkanethiol solution of

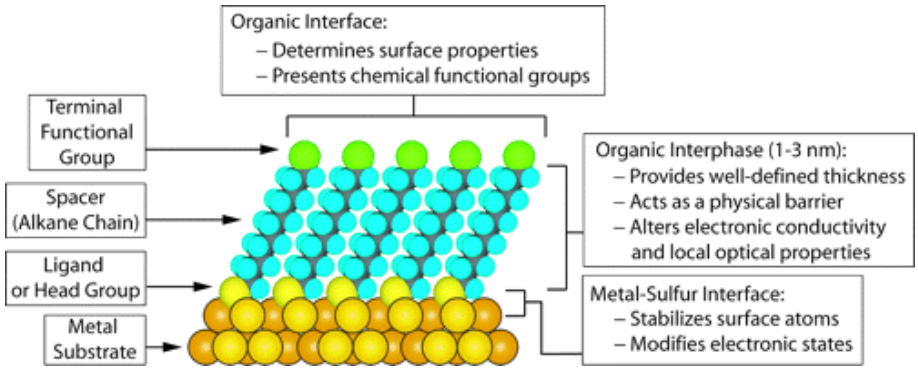

Figure 1.1: Structure of SAMs. The head group binds metal surface and the terminal functional group decides the properties of SAMs. The picture is taken from Love *et al.* by permission of ACS [10].

about 1–10 mM concentration. In a few minutes, 80–90% of surface will be covered. After this quick process, a slow reorganization occurs that completes a well-packed surface in 12–18 hours at room temperature [11].

As Fig. 1.1 [10] shows, a SAM is composed of a metal substrate, a head group that binds molecules to the metal surface, a molecular wire, and a terminal functional group. Many nanoscale applications use this self-assembly structure to change the surface properties by changing the properties of terminal functional groups [10, 17]. For example, SAMs can be used to change the properties of a surface or to prevent gold nanoparticles from coagulating with each other [18].

Molecular monolayer films prepared by self-assembly are attractive for biological applications because of the unique possibility to select different types of terminal functional groups, to serve as a detector for nanoscale observation of biological interactions [19]. For example, SAMs of alkanethiols with functional endgroups on gold are used for surfaces for the fabrication of highly efficient protein biochips and for biosensors such as surface plasmon resonance (SPR) detectors [10, 20].

One of the applications of SAMs that we are interested in is molecular electronics. The self-assembly process can lead to molecular-scale electrical junctions of molecular wires. The SAMs then act as an integral component of the charge transport: first, the molecular

components serve as a medium for charge transport; second, the ligand of the molecule makes electrical contact with the metal substrate, functioning as one electrode. At the other end of the SAMs, we can deposit a metal film [21], attach gold nanoparticles [22], or use mercury drops [23, 24].

In this work, we shall usually make the second contact via a conducting probe. The conducting probe can either be a wire (for scanning tunneling microscopy, STM [9, 25]) or metal-coated cantilever tip (for conducting-probe atomic force microscopy, CP-AFM [26, 27]). The methods will be described in Chapter 2.

1.2 Molecular Wires

Molecular wires are organic molecules that can transport electrons [5, 6]. Studies on charge transport through molecular wires have become very popular recently, owing to the possibility of applications to the molecular components for electronic devices [1, 4, 5].

There are two categories of molecular wires that have been studied: saturated alkane molecular wires and conjugated molecular wires [6]. For the saturated molecular wire, the alkane consists of saturated C-C bonds with linkers for binding to the electrode. They are considered poor-conducting wires since they have large energy gaps between their highest occupied molecular orbital (HOMO) and lowest unoccupied molecular orbitals (LUMO). The main charge transport mechanism for these wires is tunnelling: experiments show that the conductance (G) of alkanes decreases exponentially with the length of the molecule (L) [23, 27],

$$G = G_C \cdot \exp(-\beta \cdot L), \tag{1.1}$$

where G_C is a contact conductance at the junctions, and β is a decay constant varying between 0.7– 0.9 Å^{-1}. Typical conductance values for single alkanes are in range of 10 nS $\sim$ 0.01 nS (S: siemens, the unit of conductance or Mho: Ω^{-1}) as the number of hydrocarbon chains increases [23, 25, 27].

The second type of molecular wire is known as a conjugated molecular wire and has alternating double and single bonds or delocalized π electrons that can function as a wire for electron transport over long distances (> 3 nm). Since these molecules have much

smaller HOMO-LUMO gaps than alkanes, they should transport charge more efficiently. Examples include oligophene [28, 29] and DNA [30].

The charge transport mechanism in conjugated molecular wires is more complex than that of alkanes. Over short distances, the electrons can move via elastic tunnelling, using the same mechanism as alkanes. As the length of the molecule increases (> 2–3 nm), a "hopping mechanism" takes over. In the hopping process, charges hop from one site to the next available site. This process is thermally activated, and the decay of conductance with length is weak. For example, Choi and Frisbie observed that, in the case of a oligophenyleneimine (OPI), $\beta \approx 3$ nm^{-1} for OPI 1 to OPI 4 (≈ 3 nm) but was 0.9 nm^{-1} for OPI n, with $n \geq 5$ (≥ 4 nm) [28]. Here n refers to the number of units in the molecule. To show that this behavior in a long chain is from the hopping process, they measured the resistances of OPI 6 and 10 as a function of temperature and found that the resistance depends exponentially on the inverse temperature, with an activation energy of 0.28 eV [28].

1.3 Charge Transport at the Interface of Metal-molecule-metal Systems

One issue of particular concern has been to understand the mechanism of charge transport through the molecule. Although the exponential decay of conductance with length has been seen in most experiments, a comparison of the absolute conductance values found in different experiments is not straightforward. This is partly because some experiments measure properties averaged over many molecules while others measure properties of single molecules. However, even in the case of single-molecule measurements, the measured conductance values for the same molecule may vary widely [31, 32, 33, 34] because of different molecular conformations at the metal-molecule interface.

Molecular wires are composed most simply of two metallic electrodes that act as source and drain reservoirs for electrons, connected via a junction of atoms or molecules. The discrete molecular energy levels of the molecule broaden into transmitting states when they are coupled with the electrodes that become part of the continuous energy spectrum of the molecular wire, and electrons may scatter off the molecular states as they move from

one electrode to the other.

As a bias voltage is applied across the electrodes, a current may flow through the junction. A standard method for predicting such currents is Landauer theory [7], which relates the electronic current flowing through the system to the quantum-mechanical probability for a single electron to scatter elastically from one electrode to the other. For a two-terminal system, the current may be calculated as

$$I(V) = \frac{e}{h}\int_{-\infty}^{\infty} dE\ T(E,V)[f(E,\mu_s) - f(E,\mu_d)], \tag{1.2}$$

where V is the bias voltage, E the energy of the electron, $f(E,\mu)$ the equilibrium Fermi distribution, h Planck's constant and $\mu_{s,d} = E_f \pm \frac{eV}{2}$ are the electrochemical potentials of the source (S) and drain (D) with respect to the common Fermi energy E_F. Generally, one can understand charge conduction as being due to a set of channels. The coherent charge transport through a molecule can be described as a sum of all transport probabilities through all channels. This is formulated by Economou and Soukoulis (1981) and Fisher and Lee in 1981. The conductance of a molecule between two semi-infinite electrodes can be expressed as [5, 6, 35]

$$G = \frac{2e^2}{h}\sum_{i,j=1}^{N} T_{ij}(E,V), \tag{1.3}$$

where T_{ij} is the transmission probability matrix, and h is Planck's constant. Landauer theory is especially relevant for short molecules between semi-infinite electrodes. In Eq. 1.3, $\frac{2e^2}{h}$ is called the *conductance quantum* $= 7.748 \times 10^{-5}$ S, or $(12.9k\Omega)^{-1}$ and often denoted as G_0. We will express conductance values of the metal-molecule-metal systems in terms of this value.

We can write the Hamiltonian of the electron for the electron-molecule junction system as a sum

$$H = H_L + H_{mol} + H_R, \tag{1.4}$$

where H_{mol} describes the molecule itself, and H_L and H_R are the transport Hamiltonians at the left and right junctions and electrodes; in this thesis, we included the coupling terms between the lead and molecule in H_L and H_R.

The resistances that result can be written approximately as,

$$R = R_L + R_{mol} + R_R, \tag{1.5}$$

$$R = R_0 \cdot \exp(\beta \cdot L), \tag{1.6}$$

where R_L, R_R, are contact resistances, and R_{mol} is the resistance of the molecule that correspond to the respective transport Hamiltonians. The resistance increases exponentially with length, as explained in the previous section. Note that Eq. 1.6 is just the inverse of Eq. 1.1.

Charge transport properties are affected by intrinsic molecular properties such as the molecular length, gap between the electronic states of the highest occupied molecular orbital (HOMO) and the lowest unoccupied molecular orbital (LUMO), the gap's alignment relative to the Fermi level of the electrodes [32], and conformation changes resulting from the contact geometry [36].

The conductance of the junction, then, remains a topic of active investigation [31, 37, 33, 38, 39]. As Fig. 1.2 suggests, the electrical properties of each junction must be as well understood as the molecule itself. Since the voltage drop through the contact is typically comparable with that of molecule itself, the resistance from the contacts cannot be ignored. Therefore, one needs to understand the charge transport at the junction before one can understand the research on intrinsic properties of the molecule under study.

Our motivation in this thesis then is to clarify some of these crucial problems in realizing molecular electronic devices. We focus on the behavior of charge transport at junctions and the development of better molecule-electrode contacts that can transport charge efficiently and reliably in the metal-molecule-metal system.

Thus, to fulfill our objectives, we will introduce and review different experimental techniques for measuring single-molecule conductance in Chapter 2. In Chapter 3, we discuss our apparatus, the materials we use, and the values of some relevant parameters. The results that we found will be discussed in Chapter 4. In particular, we will describe three sets of experiments:

1. We report observations of conductances for three different electrode configurations with a simple molecule, 1,8- octanedithiol (ODT): Au-ODT-Au, Pt-ODT-Pt, and Pt-ODT-Au. We observe the existence of two conductance series and compare the con-

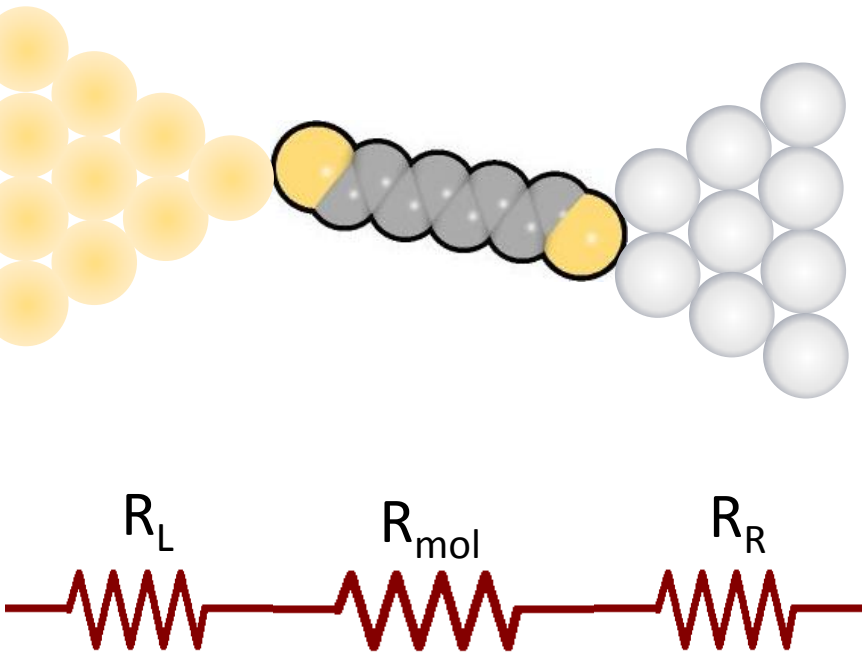

Figure 1.2: Molecular configuration in a metal-molecule-metal system and equivalent resistors, with R_{mol} the resistance of the molecule of interest and R_L and R_R the resistances of each anchoring group. The molecule depicted here is 1,8-octanedithiol (ODT, $C_8H_{16}(SH)_2$), which we used for our experiments.

ductances through platinum and gold electrodes and discuss the conducting mechanism between a molecular ligand and a metal electrode by considering binding strengths and electron paths between them.

2. We study the behavior of each of three configurations, Au-ODT-Au, Pt-ODT-Pt, and Pt-ODT-Au, as a function of the bias voltage. We observe a nonlinear current response as increasing the bias voltage due to the interface states formed at the junction [40], an effect that might be useful for manipulating electronic properties of the metal-molecule-metal system.

3. Finally, we evaluated the stability of junctions for the Pt-ODT-Au and Au-ODT-Au systems (We were not able to evaluate Pt-ODT-Pt for technical reasons that we will discuss in chapter 3.)

An ideal contact requires durability and stability while functioning. Stable molecular junctions can give more reliable conductance values since the conductance is affected by the molecular configuration changes. A method to evaluate the stability of a junction is to measure how long the junction can persist while the distance between two electrode increases. We evaluate the stability of thiol-gold and thiol-platinum junctions as a function of voltage bias, in order to determine whether there is a relation between the conductance and junction stability.

Chapter 2

Experimental Methods

In this chapter, we review techniques for measuring the conductance of single molecules and discuss their strengths and weaknesses. Basically, to investigate the conductance of single molecules, one needs two electrodes and a molecule of interest. The molecule of interest must have a linker group at each end that connects to the metal electrodes. This sounds straightforward, but in practice, it was not achieved until 1997 when Reed *et al.* first measured the single-molecular conductance of a benzenedithiol molecule using a mechanically controlled break-junction set-up [8] inspired by the initial proposal by Aviram and Ratner in 1974 [5, 4].

Why did it take over two decades to measure the conductance of a single molecule? First, there were no proper tools to measure phenomena at such small scales. Second, technological developments in microfabrication were needed.

Gerd Binnig and Heinrich Rohrer invented the STM (scanning tunnelling microscope) in 1981(at IBM Zürich) [15, 41], and Binnig *et al.* invented the AFM (atomic force microscope) soon after, in 1986 [16]. Since then, STMs and AFMs have been used to image nanoscale structures and explore nanometer-scale phenomena. Since the first single-molecule measurements of Reed *et al.*, many single-molecule studies using AFM and STM have been reported, for example [9, 25].

Various methods have been devised for measuring the conductance of a single molecule. Some of these methods measured current-voltage characteristics as averaged over a few molecules using STM/AFM [9, 27, 42, 32]; other methods reported results from a single molecule [14, 22, 33, 43]. Unfortunately, there were many discrepancies among these

methods [33].

To clarify these somewhat conflicting results, we present them below in more detail, focusing on the single-molecule measurements. We focus especially on studies concerning the binding mechanisms and their effect on the conductance of individual molecules.

One can categorize single-molecule measurement techniques into two types. First, one can measure the conductance of single molecules statically, as described in Section 2.1. In this case, both electrodes and molecules in the metal-molecule-metal system are fixed and not moved. Second, as described in Section 2.2, one can measure the conductance dynamically by moving (approaching and retracting) one or both electrodes.

2.1 Static Methods with Fixed Electrode

We present two methods for statically measuring a single-molecule conductance. The first is the monolayer-matrix-isolation method [22], and the second is the nanofabricated-gap method [14].

2.1.1 Matrix isolation using gold nanoparticle and conductive AFM

This method uses gold nanoparticles (GNPs) attached to isolated molecules of interest (typically dithiolates) in a matrix of non- or poorly conducting molecules, typically monothiolates. This method is performed on self-assembled monolayers (SAMs) that include both the molecule of interest and the matrix molecule on a substrate, typically gold.

There have been two strategies for making this type of SAM: The first is to make a SAM in a mixture of monothiol and dithiol solution. By adding a small amount of dithiol to a large concentration of monothiol, one can make a SAM of isolated dithiol molecules. A second method is to insert dithiols into a monothiol SAM by an exchange reaction. Cui *et al.* used the latter method to measure the conductance of embedded octanedithiol molecule in the matrix of octanethiol [22]. In detail, they first made a SAM of 1-octanethiol (OMT) on a gold film deposited on mica. Then, the gold substrate with OMT SAM was incubated by immersion in 1mM ODT solution. By exchange reaction, a small portion of ODT was inserted into the OMT matrix. After a thorough ethanol rinse, gold nanoparticles (GNP) were suspended into the mixed monolayer in solution.

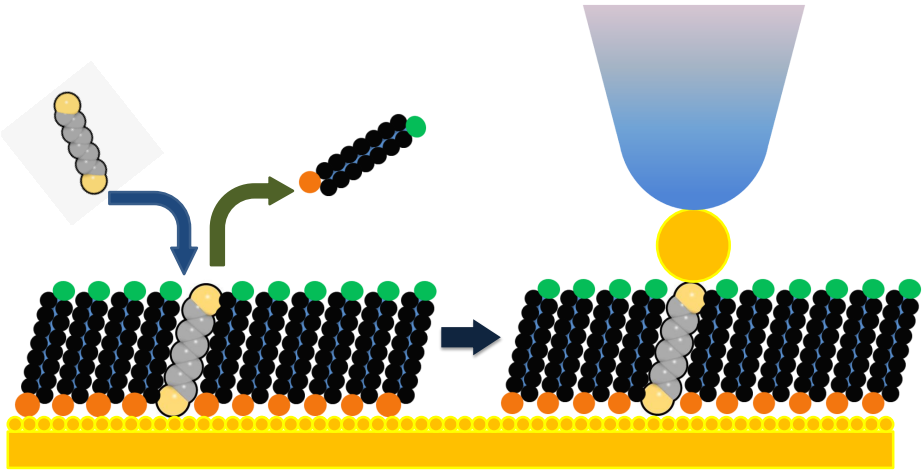

Figure 2.1: Schematic diagram of the matrix isolation method by Cui *et al.*: On a monothiolate SAM, a highly diluted dithiol solution is introduced. Isolated dithiol molecules are then formed by chemical exchange. After immersing the mixture of monothiol-dithiol SAM into a solution containing GNPs, one sees that GNPs bind to the dithiols. Then, using a conductively coated AFM probe, one can contact the GNP to measure the conductance of an isolated dithiolated molecule.

Since GNPs selectively bind to sulfur atoms of ODT and since the matrix molecules are insulators, one can consider the molecule of interest to be isolated in an insulating matrix with a GNP contact point. By constructing a histogram based on the results of thousands of molecular junctions, Cui *et al.* observed that the slopes of current-bias graphs (conductances) were grouped in families that were integer multiples of a minimum slope,They interpreted the value of the slope as reflecting the number of molecular contacts made to a GNP. From the lowest value of the slope, they estimated the resistance of ODT to be 950 MΩ [22].

Later, the same group corrected their results after considering effects due to GNP size and to contact forces between GNP and AFM tip [44]. In particular, small GNPs are sub-

ject to Coulomb-blockade effects [45], where an electron fills in the quantized states of a GNP and generates an electrostatic potential. Using larger GNPs ($d \approx 5.6$ nm) Morita and Lindsay reduced the effects due to the GNP size. They repeated the current-voltage measurements and concluded that there were two conductance values for alkanedithiols. We will discuss these two conductance values later. After these corrections for GNP size and tip force, the measured conductance for the alkanes C8 (*octane-*), C10 (*decane-*) and C12 (*didecanedithiol*) agreed quantitatively with both theoretical calculations and other experimental techniques such as the break-junction technique [46].

2.1.2 Nanofabricated gap method

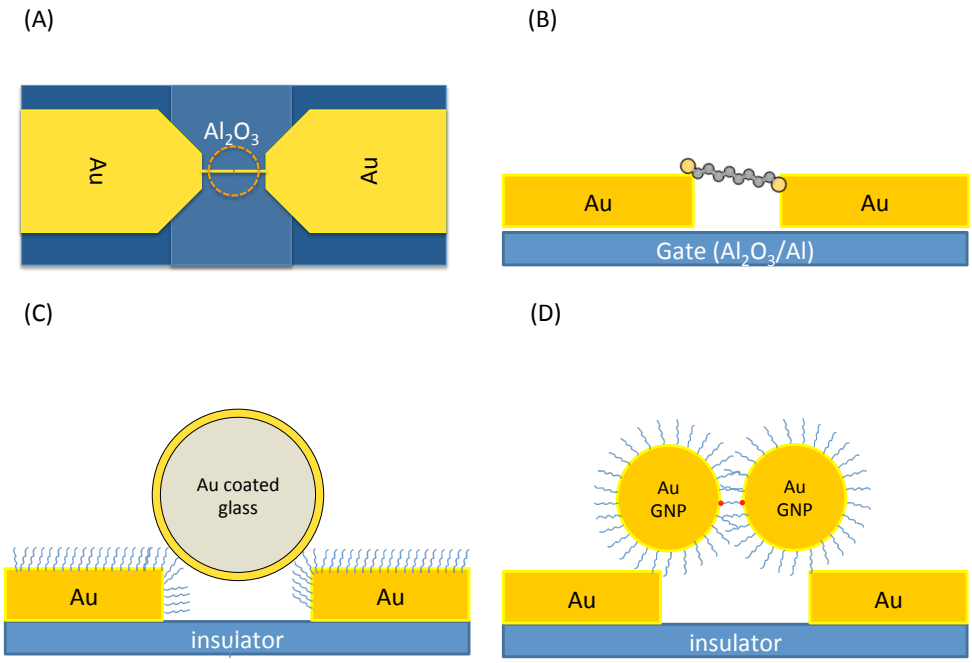

Figure 2.2: Diagram of nanofabricated gap methods: (a) A gap directly fabricated by lithography and electromigration. Sketch is similar to a set-up of Song *et al.* (b): Zoom-in view of circled area of set up (a). (c),(d): Other methods for attaching a molecule in the space of a nanometer gap. See the text for explanation.

For wiring molecules between metallic junctions, the simplest way would be to make a nanometer-scale gap between two metal electrodes. However, creating such a gap is difficult. For example, structures using conventional electron beam lithography are limited to sizes $\gtrsim 10$ nm [14, 47]. Thus, several new methods have been devised that can achieve nanometer gaps. These methods include "electrostatic trapping" [13] and "electromigration break junction" [14].

I begin with the electromigration break junction method, focusing on Park *et al.*'s fabrication method. A thin block or wire having a waist (≈ 10 nm) is fabricated by evaporation and electron beam lithography. Then, controlled bias voltages are applied through the junction in an ultra-high vacuum (UHV). The high fields created in the narrow junction are strong enough to displace atoms in the wire. Eventually, the displacement ("electromigration") leads to the formation of a small gap (1–3 nm) [14, 48, 49, 50].

The existence of gap is first checked by making sure that no electric current passes through the gap and then is verified by SEM (Scanning Electron Microscope). A highly dilute solution containing the molecule of interest is then introduced in order to make molecular bridges across the gap. The current characteristics are measured to confirm the formation of a molecular bridge.

Some methods use gold nanoparticles to overcome the difficulty of making a nanometer-size gap. In these methods, a nanometer gap is achieved either by introducing gold nanoparticle on electrodes with adsorbed molecules or by a connecting a single or a few molecules between two nanoparticles [33]. Schematic explanations of nanometer-gap formation using the two methods are depicted in Fig. 2.2 (c) and (d).

This system is close to a macroscopic device since it has a source, drain, and gate [48, 50]. One can then measure the reproducible current-voltage characteristic under the influence of the gate voltage [50]. However, it takes many trials to get a proper-sized gap. And even given a proper-sized gap, there is no direct control over how many molecules bridge the gap. Thus, both of these methods fail to allow one to study single-molecule junctions.

2.2 Dynamic Method: Break-junction Technique

The most successful method for measuring conductances of single molecules dynamically is the break-junction method. In this method, one or both electrodes are repeatedly moved into contact and retracted while a bias voltage is applied. Two widely used implementations

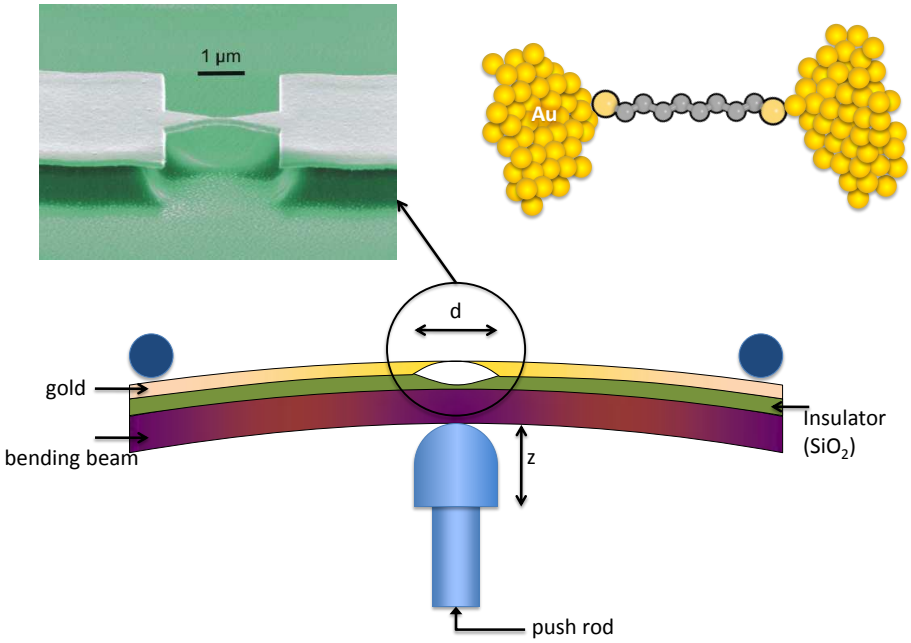

Figure 2.3: Sketch of the mechanically controlled break junction (MCBJ) technique. The push rod raises the height (Δz), thereby increasing the distance between electrode by Δd. A controllability of displacement Δd between electrodes is determined by the ratio ($\Delta d/\Delta z$). The zoom-in photograph in upper-left is the MCBJ set-up of Trouwborst *et al.* [51] by permission, copyright (2011) by American Physics Society.

of break-junction techniques have been reported. The first is the mechanically controllable break-junction (MCBJ) method [8, 52, 43, 53, 54, 55]. This method uses a thin wire or microfabricated strip of metal to form breaking electrodes. The substrate is an insulator such as a polymer. Contact and separation can be controlled by bending the substrate on which the strip is attached, as shown in Fig. 2.3. For the microfabricated beam setup, a

metallic suspension bridge structure can be achieved lithographically [53, 54, 55].

Such setups are able to create a very small displacement ratio ($\Delta d/\Delta z$) between the movement of the push rod (Δz) and the displacement of the electrode gap (Δd). For example, the MCBJ setup of Tsutsui *et al.* has $\Delta d/\Delta z = 3 \times 10^{-4}$ [56]. This displacement ratio then allows one to translate a large movement into a much smaller one. The setup of this method is simple and able to control the length between electrodes with great precision and stability, especially at low temperature [51].

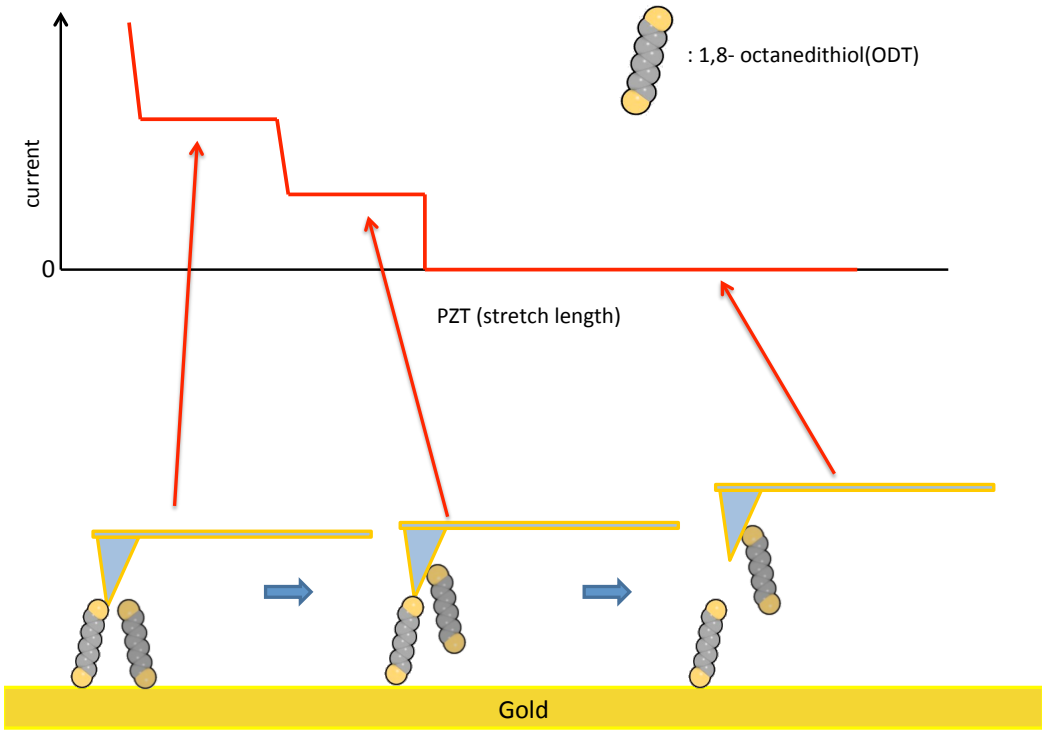

Figure 2.4: Schematic description of the AFM break-junction technique (AFMBJ): When the tip approaches the surface, it makes connections to several molecules. Under an applied bias voltage, a current-distance diagram shows conductance steps corresponding to the unit molecular conductance.

Huisman *et al.* [53] proposed and corroborated the following scenario for a break-junction experiment using their MCBJ setup: When two metal electrodes are brought into

contact mechanically in a solution containing molecules, adsorbed molecules on each electrode formed several "molecular bridges." Then, when the two electrodes are separated from each other, one observes a series of conductance steps in the current-distance graph recorded for a given bias voltage. The current data is recorded as two electrodes are brought together and separated. The experiment is then repeated hundreds to thousands of times. All of the conductance values from all the trials are collected into a single histogram. Because current steps or plateaus are associated with long runs of similar current values, the histogram will show peaks at currents where steps tend to be observed. See Fig. 2.4.

The other break-junction implementation uses a scanning probe microscope (SPMBJ), where STM tips or metal-coated AFM cantilevers measure the current while approaching toward and retreating from the metal surface repeatedly. Both methods can be carried out either in liquid [57, 58, 59, 31, 60, 37] or in ultra-high vacuum [61, 62].

Since the SPMBJ set-up measures a conductance while pulling the tip out of the surface, we are easily able to observe the different conductance values as the configuration between the ligand and metal electrode changes.

There are also variants of SPMBJ. Haiss *et al.* developed the "*I(s)* method," which avoids direct contact between the tip and the surface. Instead, as the STM tip approaches the substrate, the electric field between the tip and the substrate draws up a molecule lying on the substrate and makes a molecular contact with the molecules that span the gap between tip and substrate [63]. This technique needs a low-coverage monolayer (low concentration of molecules on surface) to allow a free reorientation of the molecules near the tip's contact point. Only one or two molecules can be drawn to the SPM tip when it approaches. Haiss *et al.* further observed that the molecular conductance can be determined from the magnitude of the switching telegraph-noise-like currents that pass through the trapped molecule between the tip and substrate [64]. Here the tip-substrate distance should be slightly less than the length of one molecule. These variation of SPMBJ have some advantages however, these methods require much precise measurements and instrumentations [65].

These break-junction techniques have been the most successful in obtaining measurements of conductance for single molecules that correlate with theoretical expectations. A particular advantage of the break-junction methods is that they are fast and allow one to make a large number of observations. One can then infer the measured relative likelihoods

of different types of bonds or junctions.

In addition, since the geometry of the molecule-electrode junction can vary every time the molecule makes contact with the electrode, the electric behavior of a junction due to the binding configuration can be determined by this method. Thanks to this characteristic, many observations of different conductances because of geometric junction changes have been reported using the STMBJ.

For example, Li *et al.* [31] observed two conductance series, a high conductance (HC) and a low conductance (LC) series. They explained the existence of a series of conductance values as reflecting the possibility for n molecules to bridge the gap between the gold electrodes on both sides of the alkanedithiol [31]. Haiss *et al.* observed three different series of conductance values [34]. The existence of two or three conductance values for alkanedithiols between gold electrodes is now generally accepted [66, 67]. We also found three different series of conductances in our measurements, as we will discuss in detail in Chapter 4. Our interpretation, however, will differ from that of Li et al. [66]. To keep the discussion simple, we will follow the notation of Li *et al.* for the names of these three series (HC, MC, and LC). In this thesis, we chose the break-junction method since this method can measure different types of electric behavior at the junction between molecule–electrode in spite of issues connected with the broadening of histograms due to molecular elongation [68]. We determined conductance series for 1,8-octanedithiol between a gold and a platinum electrode using the break-junction method.

Generally, each method has its own strengths and weaknesses. Static methods can measure one specific binding many times allowing the measurement of complete I–V curves. In addition, if a device using a single molecule has to be made, the device will be built using a static set-up similar to the static methods we mentioned. However, the break-junction method enables us to investigate microscopic challenges that the static methods have, such as contact geometry, current-induced instability and local heating [6]. A completely satisfactory measurement technique has yet to be developed.

Chapter 3

Description of the Experiment

In this chapter, we present details of our experimental setup, including the apparatus itself, sample preparation, sample characterization, and data analysis.

3.1 Apparatus

For our break-junction experiments, we used a commercial atomic force microscope (Asylum Research, Model MFD-3D). The break-junction experiment was performed in a closed liquid cell. The closed liquid cell is composed of a closed-cell dish made of PEEK (polyether ether ketone, a chemically resistant plastic), a glass window, sealed hole for a metal electrodes for contact, a flexible viton membrane, and O-rings. These were cleaned thoroughly in ethanol and deionized (DI) water by sonication. They were then dried with filtered pure N_2 gas (99.99%, Praxair Co.) before each experiment to prevent contamination while assembling the closed liquid cell.

We used a cantilever holder for AFM having a dual-gain amplifier. This amplifier collects current through the tip simultaneously with a high-gain (1 nA/V) and a low-gain (1 μA/V) I–V converter. The transformed signal is converted to a digital signal by a 16 bit A/D converter at 200 kHz. The maximum acquisition rate we could select via software was 50 kHz.

We used Au-Cr and Pt-Ti coated cantilevers with spring constants ranging from 0.6 nN/nm to 36 nN/nm (nominal values from the manufacturer). To measure the force exerted while breaking an Au junction ($\approx 1.5 \pm 0.2$ nN [59]), we need to make sure that the

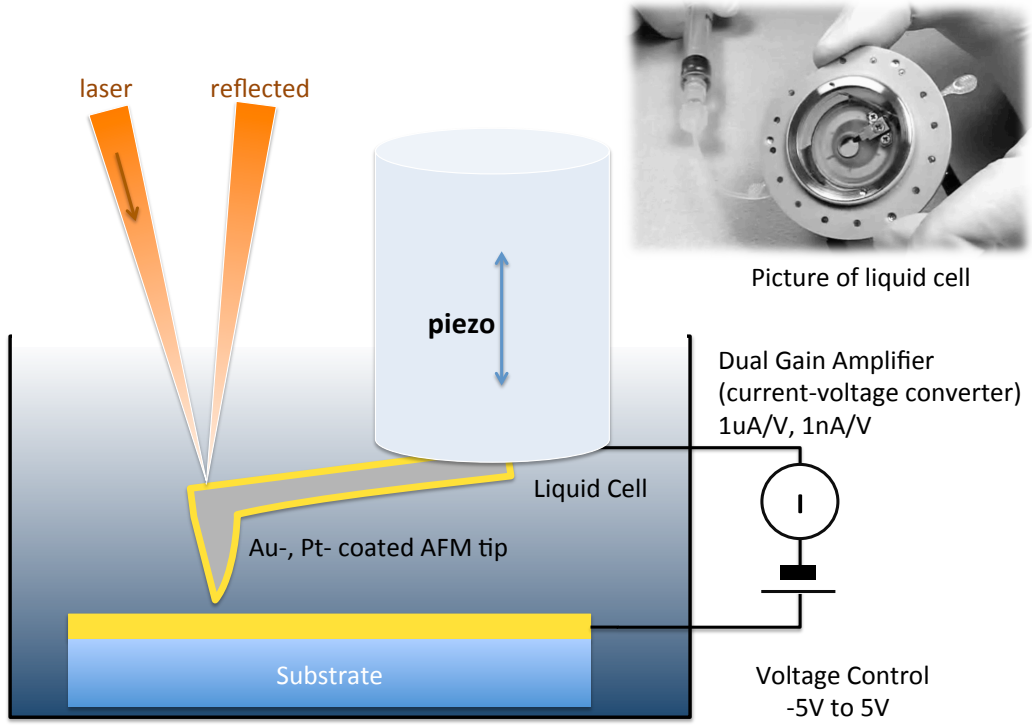

Figure 3.1: Schematic diagram of conductive-probe AFM measurement and photograph of the cell. A conductively coated cantilever coated with Au or Pt is brought into contact with a substrate in a closed liquid cell. The inset is a picture of the closed liquid cell (Asylum Research Co. Part No. 939.009.). The voltage is applied between the substrate and the conductive cantilever, and the current signal is amplified using a dual-gain amplifier and then digitized. See text for details.

deflection of the cantilever is comparable to the force exerted so that the deflection can be measured with a good dynamic range. We used both relatively soft cantilevers ($\approx$ 3 nN/nm) and relatively hard cantilevers ($\approx$ 36 nN/nm) for conductance measurements. The spring constants did not affect the conductance values.

3.2 Break-junction Technique with AFM

The break-junction technique using scanning probe microscope (SPMBJ) has several strong points for conductance measurements of single molecules. First, this technique has proven effective for determining conductances of single molecules [57, 69, 37]. Second, the method allows one to analyze effects due to the binding geometry between a molecule and a metal electrode [59, 31, 54, 70].

We used the conductive AFM or conductive-probe AFM technique (C- or CP-AFM) for repeatedly breaking molecular junctions at the sample surface. The C-AFM technique has been widely used for measuring the conductance of molecules in SAMs [21, 27, 71]. A disadvantage of this method is that one does not measure directly single-molecular conductances. The matrix-isolation method is better for this aspect, as we discussed in the previous chapter (Sect. 2.1). However, the break-junction techniques combined with AFM are able to measure the current through a single molecule, while at the same time measuring the force exerted when the single-molecular bond ruptures [59, 60, 54]. In addition, since the AFM can image the surface before and after break-junction measurements, one can easily track changes to the surface resulting from the measurement itself.

3.2.1 Measurements

The important parameters for break-junction measurements of electronic and mechanical properties of a single molecule are the bias voltage, retraction speed of the tip, and spring constant of the cantilever.

We carried out measurements under bias voltages ranging from 0.05 V to 0.8 V. The bias voltage is applied to the substrate via the AFM head power supply. The current through molecules flows through conductive tips to the dual-gain current-to-voltage converter located inside the cantilever holder.

For the Pt-ODT-Pt configuration, we were not able to carry out the measurements as a function of bias voltage. Because of the high conductance of Pt-ODT-Pt, bias voltages greater than 0.2V implied currents larger than 10 nA, the high-gain limit of the dual-gain converter. As a result, we were unable to compare high-bias conductance values directly with other configurations. We do, however, report measurements done at a bias voltage of 0.1 V.

We used cantilever retraction speeds ranging from 10 to 200 nm/s. Since the junctions we study break-junctions during tip retractions, we used an approach speed several times faster than the retraction speed both to make a good initial contact between the metal tip and metal-coated substrate and also to reduce the overall measurement time.

We performed break-junction measurements both in ODT solutions and on ODT SAMs in hexane solvents. There were no significant differences in the conductance currents measured in the two situations. When measuring conductance in a 1mM ODT solution, ODT SAMs are formed both on the substrate and on the tip continuously. By contrast, ODT SAMs were initially formed only on the substrate in the latter case. In the break-junction measurements on ODT SAMs, we made an ODT SAM on gold and Pt film by immersing for 24 hrs in a 1mM ODT solution. Then we conducted break-junction measurements in a hexane solvent.

3.2.2 Stretch-length analysis of current-distance curves

As Fig. 3.2 shows, we observe conductance plateaus when the AFM tip stretches out the molecule before it ruptures. We use the "stretch length" as an indicator of the mechanical stability of the bonds between the molecule and the tip and between the molecule and the Pt and Au substrate. We measured stretch lengths from conductance plateaus collected from all current traces of the break-junction measurement.

The method we used to measure the stretch length is described in Fig. 3.2. First, we construct the conductance histogram to determine the locations of the peaks (HC, MC). Then, we set the range for the HC as $I_{HC} \pm 10\% \times V_{bias}$, ($\approx$ 0.2 nA) and for the MC as $I_{MC} \pm 10\% \times V_{bias}$, ($\approx$ 0.04 nA) at $V_{bias} = 0.1\ V$. We keep this range fixed for all the other bias voltages by dividing by the ratio of the bias voltage to 0.1 V.

Then, we find x values (piezo) corresponding to the upper limit (x_{up}) of the range from

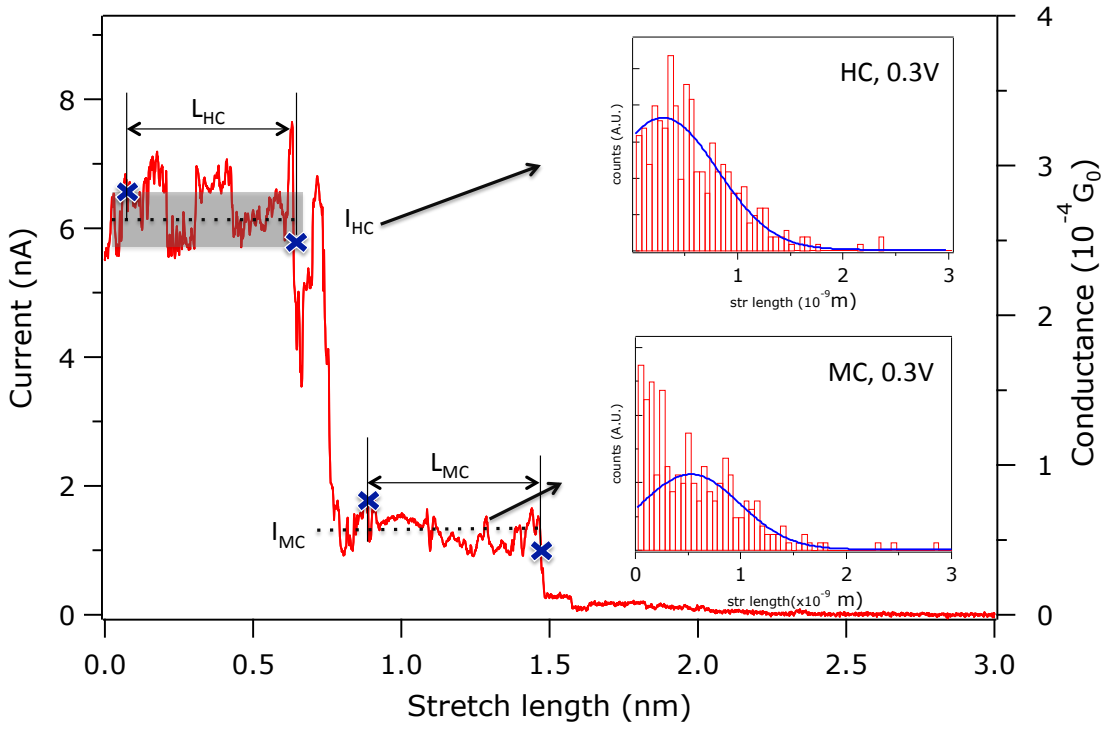

Figure 3.2: Determination of HC and MC stretch lengths. Example of data taken on ODT. The main graph shows a current-distance graph. The inset graphs are stretch-length histograms. See the text for a detailed explanation for how we determine stretch lengths. I_{HC} denotes the current corresponding to HC. (X) marks are upper and lower range of set currents and a shaded region is an acceptable range set by the calculation ($I_{HC} \pm 0.2$ nA, $I_{MC} \pm 0.04$ nA, see text for detail). Inferred lengths are denoted as L_{HC}, and L_{MC}.

the start and the x values corresponding to the lower limit (x_{low}) of the range from the end. The points that we found in Fig. 3.2 are marked (X). To check the validity of the length, the mean value (M) for the range is calculated and compared with I_{HC} and I_{MC}. If the mean value exceeds the limit by more than $\pm$ 20 % of the original value (the peak location), e.g., if $\frac{|M-I_{HC}|}{I_{HC}} \geq 0.2$ for HC, then we find the next x values matching the upper or lower limit, depending on whether the mean value is located below or above the limit. After finding the x values for the range, we set the stretch length to Δx, corresponding to the difference in distances between the x_{up} and x_{low} ($\Delta x = |x_{\text{up}} - x_{\text{low}}|$). This procedure is carried out automatically using a code written for Igor PRO (Wavemetrics). Then we compiled the measured lengths into histograms and fit Gaussian curves through them to infer stretch length values. In Ch. 4, we discuss the possible significance of statistically significant deviations of the histograms from Gaussian curves.

3.3 Sample Preparation

3.3.1 Gold and Platinum Substrate Preparation

We prepared gold and platinum thin films on mica and plasma-cleaned glass slide substrates, to serve as metal electrodes for metal-molecule-metal systems.

The platinum substrates were prepared by electron-beam evaporation on glass slides (Fisher Scientific, thickness # 2) at the 4D LABS at Simon Fraser University. First, glass slides were cleaned by *in situ* Ar-plasma at 100 W, 4×10^{-3} torr, for five minutes. Then a Cr adhesion layer (~ 5 *nm*) and a Pt layer (~ 200 *nm*) was deposited at 0.7 to 0.9 Å/s. These evaporations were performed by Chris Balicki, a technician at 4D LABS.

For gold deposition, I evaporated gold (99.99%, PAMP S.A.) on freshly cleaved mica by thermal evaporation at 380 $\pm$ 5 °C. The deposition rate was 0.5 Å/s, and the base pressure was less than 2×10^{-6} torr. I kept the substrate temperature at 380 °C for more than 7 hours before and 3 hours after evaporation to remove impurities from the mica surface and to give enough time for adsorbed gold atoms to move and create a flatter surface.

As we see in Fig. 3.3, the gold on mica has large, flat grains, but the platinum surface has small grains. This difference in flatness results from different deposition conditions and the much higher melting temperature of platinum, (1770 °C) relative to gold (1065 °C).

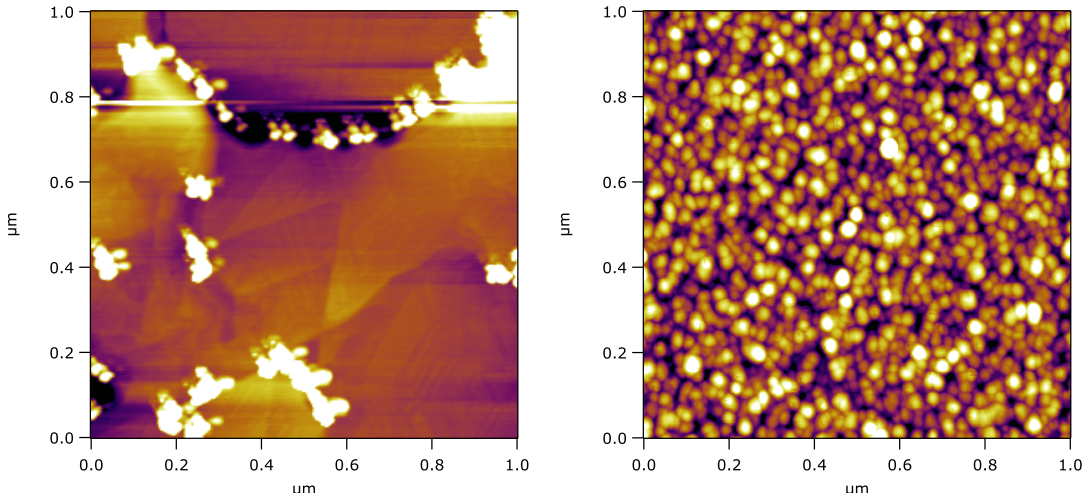

(a) AFM image of annealed surface of Au (b) AFM image of annealed surface of Pt

Figure 3.3: The AFM topography of Au (111) and Pt. The grain size of platinum is far smaller than that of gold because of deposition conditions and a higher melting point.

After evaporation, films were kept in a vacuum desiccator. Just before each experiment, every film was cleaned for 20 minutes by UV/O_3 cleaner (Novascan, model: PSD-UV) and briefly annealed using a butane flame torch. When annealing the film, I observed the outer flame in the dark so that the film glowed dimly with an orange color for 1 minute. I carefully waved the flame up and down at about 1 Hz in order not to roughen the surface. The important point is that since gold does not wet mica, liquid gold gathers into small droplets, creating a rough surface. Thus, while annealing allows surface to become smoother, melting roughens it. The procedure described above thus tries to ensure uniform temperature, to avoid any local melting.

3.3.2 Chemicals

We used 1mM of ODT solution of hexane for making ODT SAMs and performing break junction measurement. 1,8-octanedithiol (ODT) was purchased (98%, Alfa Aesar). ODT is composed of eight CH_2 groups with thiols (-SH) at each end of the molecule, as shown in Fig. 1.2. ODT is a good model system for investigating of conductance properties of contacts, for several reasons. First, the sulfur atom has a strong affinity for the noble metals,

including gold and platinum. Second, because alkanes have large HOMO-LUMO gaps, electron tunneling is the main conduction mechanism through ODT. This property enables us to consider the sole effect of the contact in isolation from the complexity of molecule itself. Finally, since ODT is one of the most widely studied alkanedithiols, its conductance has already been measured. These properties led us to choose ODT to investigate the metal-ligand contact.

While various anchoring groups such as thiol (-SH) [72, 31, 58, 54, 55], amine (-NH_2) [37, 72], phosphine (-PMe) [72], and carboxylic acid (-COOH) [38] have been studied, we chose the thiol linker because it shows a higher conductance and because we can compare the conductance for the Pt-ODT configuration with previous results on the Au-ODT configuration [11, 27].

For a solvent for the ODT solution, we tested hexane (EMD, 98.5%, HPLC grade), 1,2,4-trichlorobenzene (TCB, Alfa Aesar, 99%, spectroscopy grade) and toluene (Anachimia, 99.5%, reagent grade). We preferred hexane because, among the solvents tested, it had the least effect on the viton membrane of the liquid cell. With other solvents, I hardly ever saw the saturated currents ($= 10\ \mu$A) that indicate direct contact between the tip and the metal substrate. In addition, I saw many steps or smooth decrease in current-distance curves, which I believe are artifacts because the steps do not correspond to a known conductance of ODT. A smooth decrease of a current means the existence of layers that conduct current other than a ligand-to-ligand conduction through ODT.

We believe that the observed contamination is due to the greater reactivity of toluene and TCB relative to hexane. For the case of TCB, since the Pt electrode can bind the Cl of TCB, we are not able to measure conductance of ODT, because of a layer of TCB.

In addition, the current noise level of hexane itself is the lowest among the three solvents. I ascribe this observation to its low dielectric constant (1.88 at 25 °C, vs. toluene 2.38, trichlorobenzene 2.24, at 20 °C). In general, the dielectric constant of solvents are related to the solvent polarity. A high polarity can result in fragmentation of a solvent molecule resulting from the high electric field concentration between the AFM tip and the metal surface ($\approx 10^8$ V/m).

Hexane has the disadvantage of a higher vapor pressure; however, the closed liquid cell chamber minimized evaporation. In practice, I could perform measurements for several hours.

3.4 Statistical Analysis

For each measurement, I collected several hundreds to several thousands of current-distance data. I compiled the data into histograms with selected bin sizes and ranges. We keep the bin size fixed in current scale ($\approx 7.748 \times 10^{-12}\mathrm{A} = 10^{-6}\mathrm{G}_0$ at 0.1 V). I set $1 \times 10^{-5} G_0$ as the lower limit of the log-log histogram graph. The general procedure for break-junction measurements is described in Sect. 2.2.

I collected all the data, except for trials where the current never reached the saturation level of the high-gain amplifier (10 nA). In those cases, we infer that the tip never came into full contact with the several molecules on the substrate. Finally, to compare histograms on a similar scale, we divided each histogram bin value by the number of current traces collected.

Chapter 4

Results

4.1 Conductance Measurements of ODT Bound to Gold and Platinum Electrodes

To explore the conduction mechanisms at the Pt and Au electrode, we first measured the conductance of ODT on Au. Since the conductance of ODT on an Au electrode has been reported previously [59, 57, 31, 66], we can compare our data with that of others. We measured the conductance of ODT for Au-ODT-Au using the break-junction technique (Ch. 2.2). Then, using the same technique, we measured the conductance of the Pt-ODT-Au and the Pt-ODT-Pt (tip-molecule-substrate) systems and compared their conductances with that of the Au-ODT-Au system.

Table 4.1: Conductance comparison of Au-ODT-Au, Pt-ODT-Au, and Pt-ODT-Pt system of histogram peak location for V_{bias}= 0.1 V. Conductances are in units of $10^{-4}G_0$.

Configuration	Au-ODT-Au	Pt-ODT-Au	Pt-ODT-Pt
HC ($\times 10^{-4}G_0$)	2.55 ± 0.2	2.8 ± 0.14	6.3 ± 0.2
MC ($\times 10^{-4}G_0$)	0.55 ± 0.05	0.65 ± 0.05	0.9 ± 0.1

The histograms of each configuration are shown in Fig. 4.1. The locations of peaks are denoted by arrows, and their values are listed in Table 4.1. All of the measurements were carried out at 0.1 V bias, with a retraction speed of 50 nm/s.

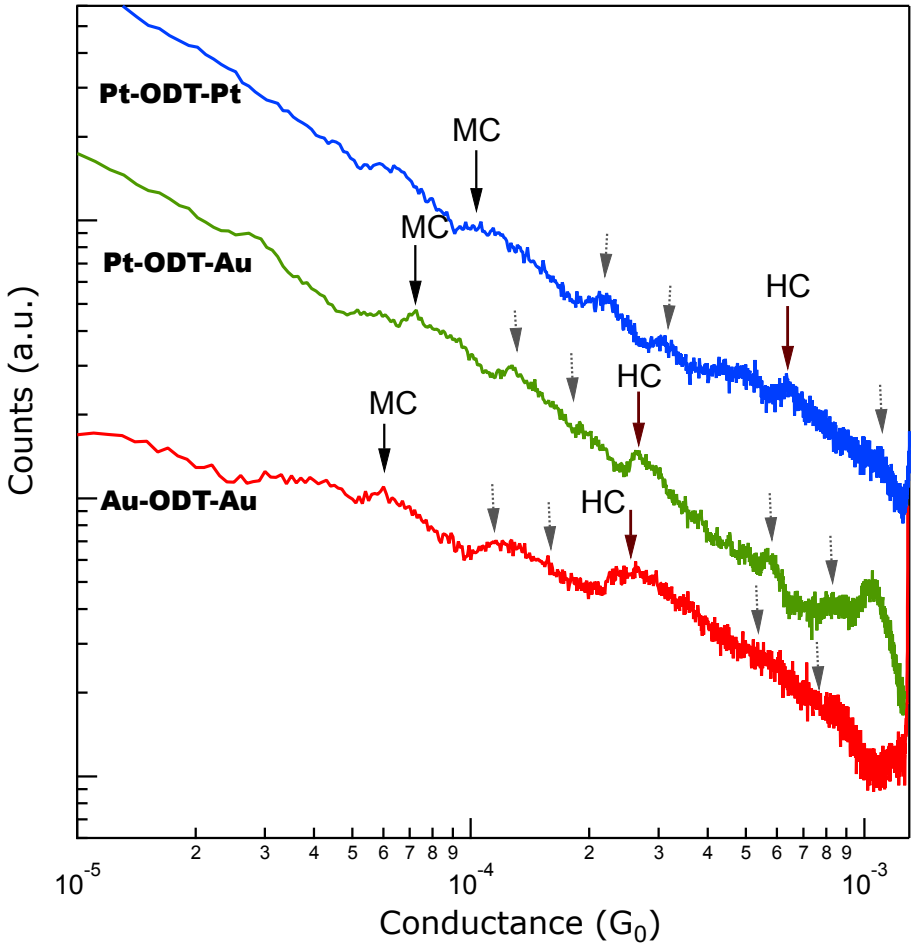

Figure 4.1: Conductance histograms of ODT for the Au-ODT-Au, Au-ODT-Pt, and Pt-ODT-Pt configurations at 0.1V. The arrows indicate MC and HC locations for the Pt-ODT-Pt, Pt-ODT-Au, and Au-ODT-Au systems. There are smaller peaks indicated on the integer multiples of HC and MC.

As we can see in Table 4.1 and Fig. 4.1, we observed at least two kinds of conductance series. We observe a number of peaks in the histogram. The two strongest peaks, indicated by arrows in Fig. 4.1 are in positions consistent with previous observations of the HC and MC state (Au-ODT-Au: MC: 0.5×10^{-4} G_0, HC: 2.5×10^{-4} G_0) [59, 31, 34]. The other peaks were difficult to localize but are qualitatively consistent with previous observations of peaks at integer multiples. In addition, we could not confirm the location of LC peaks.

As these sets of conductances have been seen previously, the approximately integer multiples of peak locations are interpreted as resulting from having multiple molecules span the gap between tip and substrate, as in Fig. 2.4 [31, 38, 73, 46].

4.1.1 Background removal

As one can notice from Fig. 4.1, the baseline of the histogram is linear in the log-log plot, and the HC and MC peaks are relatively small compared to the level of baseline.

One of the difficulties in measuring conductances of single molecules using the break-junction technique is the variation of conductances resulting from differences in the microscopic molecular binding structure between the electrode and the molecule [74, 61, 62]. This variation includes various binding possibilities for the thiol-gold binding [74] and various conformations of the molecule (*trans*: *gauche* isomer) [61, 62, 66]. These variations become more pronounced as the number of current traces increases. Under such conditions, the peaks become indistinguishable, except for the most probable peak [37, 75].

To find a way to increase the signal-to-noise (S/N) ratio for these histograms, we carried out control experiments, first, in hexane with a bare gold substrate, and then, in hexane with a 1-octanethiol (OMT) SAM on a gold substrate. We performed the break-junction measurements under identical conditions, with the only difference being the nature of the substrate. From observations of OMT and the bare gold histogram, we conclude that the part of the conductance results from contributions other than the conductance from the head to tail of ODT. Therefore, we were able not only to confirm that the peaks in ODT histograms are from ODT contacts but also to make the peaks stand out more by subtracting or dividing the ODT histogram by a background histogram compiled for these control experiments. We show the Pt-ODT-Au 100 mV histogram after dividing by the OMT histogram in (b) in Fig. 4.2. In Fig. 4.2, the MC and HC peaks of ODT have a higher

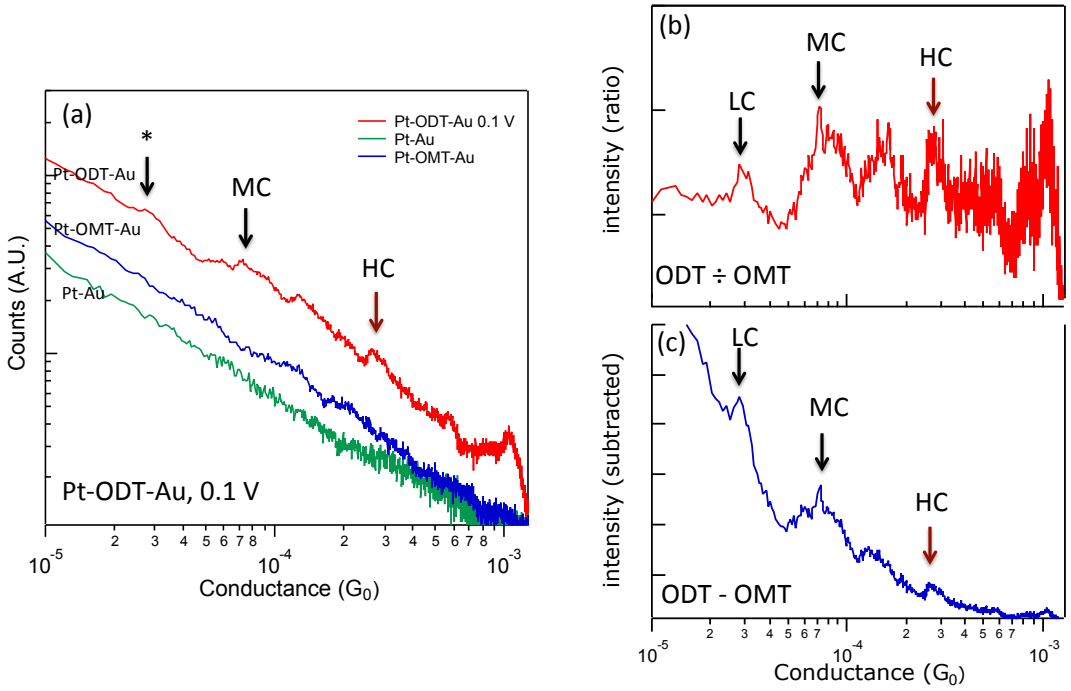

Figure 4.2: Conductance histograms for the Pt-ODT-Au configuration with control experiment, for V_{bias}= 0.1 V. (a) The top curve is the histogram of Pt-ODT-Au, while gray and dark lines correspond to histograms of control experiments performed in hexane solvent on bare gold and OMT SAM. The graphs are normalized and offset to show them clearly. Note the unidentified peak-like feature (*). (b) A histogram of ODT divided by OMT (blue) histogram. (c) The histogram subtracted by OMT histogram. Peaks in (b) stand out more than those in (c).

amplitude, and we can now confirm a third peak, LC near 2.5×10^{-5} G_0.

The histograms of both Pt-OMT-Au and Pt on bare gold are almost linear on a log-log plot, except for small peak-like features. A power-law fit gave exponents of 0.66 ± 0.01 and 0.57 ± 0.01 respectively. Generally speaking, we expect that tunneling current dominates and thus that the background histogram should be an exponential, and not a power law. However, the shape of the baseline in the current histograms is almost linear in log-log plot, indicating a power law.

Among possible hypotheses we considered, we noticed that the current-drop arises even though another part of a tip is still contacting the surface. That means, in addition to the link between each the end of ODT molecule, currents can flow through other paths, as illustrated in Fig. 4.3.

As a result of repeatedly making and breaking contact with the molecular SAM surface, an AFM tip used for the measurements becomes worn, and the metal coating at the tip is removed. Thus, an insulating material (typically doped silicon) is revealed. There then needs to be much more tip deflection in order for the conducting part of the tip to contact the molecule. Thus, there is an unknown deflection offset added to the signal for each molecule. In effect, the deflection of the tip does not correlate directly with the force applied to the molecule. In addition, there is a smaller geometric effect that makes the relative force exerted on the molecule uncertain, as well. Although we cannot find the exact force exerted on the molecule, the current-distance curves still represent the effect of pulling with increasing amounts of force.

There could be many possible reasons for such a power-law dependence— hydrogen between a tip and Au substrate [76], tunneling through solvent material, and so forth. However, none of these lead to the power-law decay. We can eliminate effects from other current paths by carrying out the break-junction measurements on densely formed SAMs. One possibility that is always present is intermolecular chain-to-chain tunneling [77, 78, 79], where in addition to the conduction mechanism through one ligand to the other, the load from an AFM tip changes the bonding structure between molecules layer and the substrate and may open additional tunneling channels through neighbouring molecules. Intermolecular chain-to-chain tunneling is illustrated in Fig. 4.4.

Wold *et al.* reported that they observed two distinct power-law relations [i.e., $R_\alpha - (\text{load})^n$], where R_α is a resistance at initial force, 2 nN) between the junction resistance and

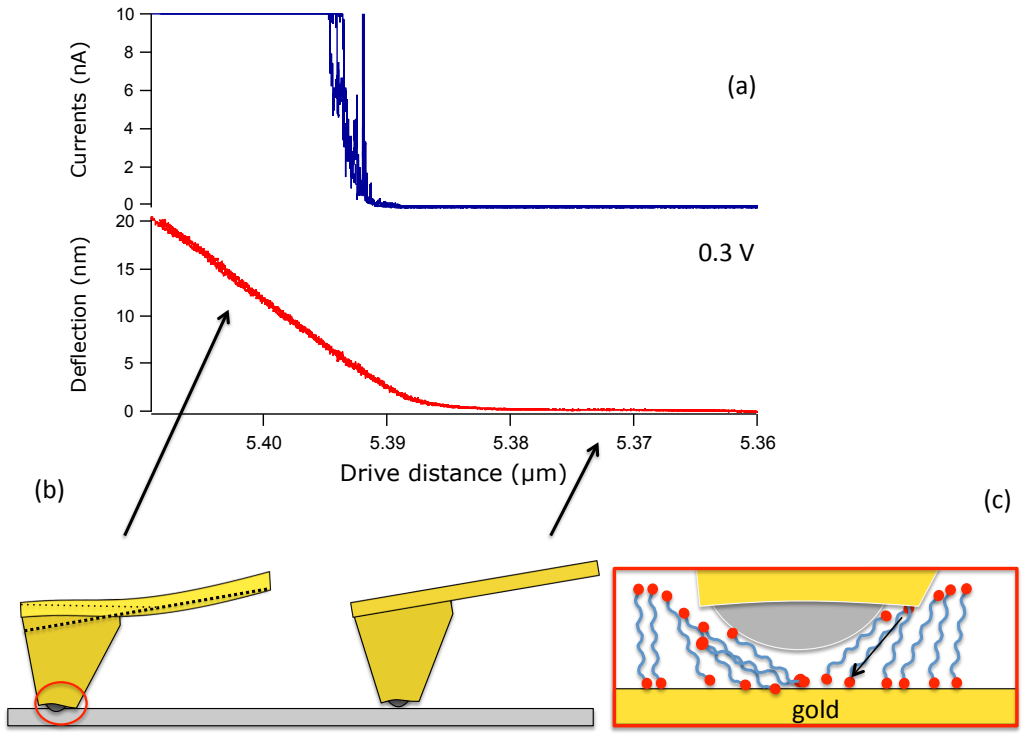

Figure 4.3: Force applied to molecules does not necessarily equal that applied to the cantilever. (a) Top: Typical current-distance graph. Bottom: Graph of deflection-distance on top. (b,c) As the AFM tip apex becomes worn and the insulating silicon is revealed, one needs more force for the conductive part of AFM tip to contact an ODT molecule, as illustrated at the macroscopic level in (b) and at the microscopic level in (c). The spring constant was k = 32 nN/nm. Since the current drop arises in the middle of AFM tip deflection, there can exist other paths for charge transport.

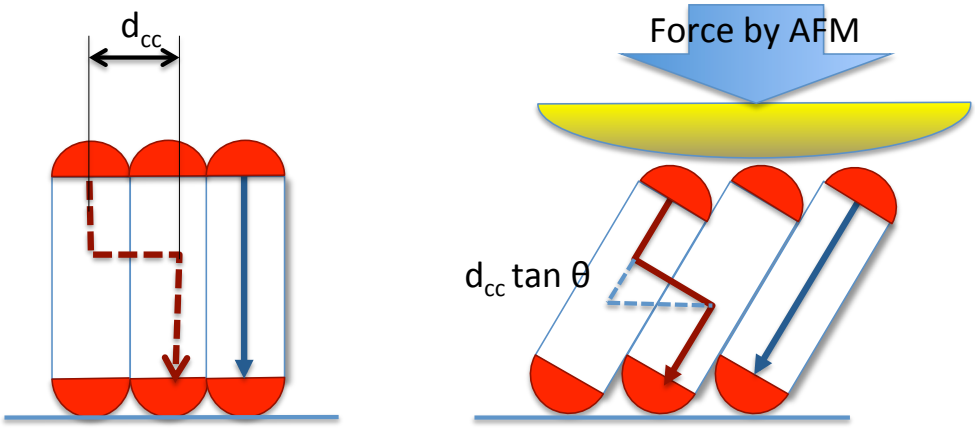

Figure 4.4: Diagram of illustrating intermolecular chain-to-chain tunneling [79, 77, 78]. Without pressure from AFM tip, ligand-to-ligand tunneling is dominant. As a pressure is applied and molecules are tilted, intermolecular tunneling becomes stronger as a path is shorten by $d_{cc}\tan\theta$, where d_{cc} is a distance from chain to chain.

the load for dodecanethiol ($CH_3(CH_2)_{11}SH$). They observed that when the force applied by the cantilever was less than 70 nN, the power n was -0.83 and when the force is greater than 70 nN, n was -7.5 [26].

Qi *et al.* reported that conductance of C16 (hexadecanethiol) increased with tilt angle of the molecule as the loading force was increased during the acquisition of I–V curves of C16 [80, 81]. Song *et al.* claimed that a tunneling current through stacked or tilted molecules resulting from the force exerted by the AFM cantilever tip affects the conductances of a whole set of molecules [79]. Their claim was based on calculations by Slowinsky *et al.* [77, 78]. They concluded that the tunneling current should increase with increasing loading force.

However, intermolecular tunneling alone cannot explain the power-law dependence of a histogram, because a histogram on bare gold also was almost linear on log-log plot. Although other studies also showed power-law backgrounds for conductance histograms [37, 82, 83], all the most obvious mechanisms – an H atom trapped between tip and substrate, tunneling through solvent material etc.– suggest that the background should be ex-

ponential. Of course, summing exponentials of different decay constants can lead to an approximate power-law decay. But we would still need to understand the robustness of the power-law. We do not know of a completely satisfactory explanation yet.

To conclude this section, first, we can effectively remove the background from an ODT conductance histogram by dividing by the OMT histogram, thereby making peaks stand out more over the background. Second, although intermolecular chain-to-chain tunneling might be a factor to explain the linearity of log-log plots of conductance histograms, but it is unlikely to be the whole story.

4.1.2 Binding Differences between the Pt and Au Electrodes

The conductance values in Table 4.1 remain constant for low bias voltages (< 0.4 V). The largest values are observed for the Pt-ODT-Pt configuration. This is as expected, since the higher work function of platinum results in a lower contact resistance, relative to gold [27]. Both HC and MC values were about twice as large as those of Au-ODT-Au. The conductance of the Pt-ODT-Au was between that Au-ODT-Au and Pt-ODT-Au, but its values, 2.8 and 0.65 $\times 10^{-4}$ G_0 were lower than median value between the Au-ODT-Au and Pt-ODT-Pt. The reason for this is related to how the Pt-ODT-Au configuration forms and that will be discussed later in the section.

How can we explain the existence of these two series of conductances as well as the observed conductance values from various metal electrode configurations? Is there a more universal explanation for the charge-transport mechanism at the junction between a metal and a molecule?

To address those questions, we first considered the differences in geometric configuration between the HC and MC conductance series. The variation in conductance is thought to be due to different geometric binding configurations. Two similar scenarios have been proposed:

The first is by Li *et al.* [31], who attributed the HC and LC (in this thesis: MC value) conductances to the binding sites of a sulfur atom at the end of the molecule. They noted that the thiol linker generally binds to three gold atoms when the ODT fills the hollow site of substrate, as when a substrate forming SAMs. When the junction is formed with the tip, and pulled out of the junction, They proposed that there are two types of binding

configuration: Hollow-molecule-top (HC), and top-molecule-top (LC) of an Au atom (See (b),(c) Fig.4.5). When an AFM tip is pulled away from a junction, the Au atom can slide up to make a top-molecule-top configuration, which corresponds to the LC case. When a sulfur of a thiol linker binds with three Au atoms, the charge can move via three different channels to the electrode. By contrast, charge has but one channel when the sulfur atom contacts the top Au atom. Thus, they claimed HC shows a conductance that is four to five times higher than that of LC, a factor that is the same as our results.

The second proposed explanation is that the the conductance values depend on the distances between metal electrodes. Haiss *et al.* carried out a modified break-junction technique called the *I(s)* technique to define the conductance of single molecules [63, 34]. Their method uses immersion in a much-diluted ($\approx 10^{-6}$ M) solution for a short time (1–10 s) to make self-assembled layers of alkanedithiol molecules which lie on the Au surface. As an STM tip under relatively high bias (≈ 0.6 V) approaches one end of a molecule lying on an Au surface, the molecule can be drawn to the STM tip and show a sharp current rise at close distances between the electrodes. Then, when the tip is pulled out of the surface, a sudden current drop corresponding to single molecule conductance is observed. They measured the current-drop heights and compiled them into a histogram. They observed three different conductance series–A, B, and C, which they associate with three possible distances between electrodes [84].

We believe that both the number of transport channels and the distance between electrodes should be considered in explaining the charge transport mechanism at the junction with different metal electrodes. Besides these, we note one more aspect: If the molecule binds to three metal atoms, as in the hollow site, not only should the distance between electrodes be closer, but also the distance between the sulfur atom of the linker and individual gold atom should be closer than the distance when the molecule is on top of the gold atom. Naively speaking, the three gold atoms draw the sulfur closer, with three times more binding force. Therefore, the HC conductance is about five times higher than MC both because of the closer sulfur-gold distance and because of having three channels of electron transport rather than just one.

Furthermore, the same reasoning can help us understand the differences between the conductances measured on platinum and on gold electrodes. We measured higher conductance values for Pt-ODT-Pt and Pt-ODT-Au than for Au-ODT-Au (See Fig. 4.1). Since

platinum has contributions from its 5d orbital [85, 67], two possible electron channels are involved for charge transport through the thiol-Pt junction. In addition, the adsorption energy of platinum is about 0.1eV lower than gold at each configuration (top and hollow) [67]. This difference implies that the platinum electrode draws a sulfur atom strongly to it [86, 87] and that the distance between sulfur and platinum is smaller than that between sulfur and gold.

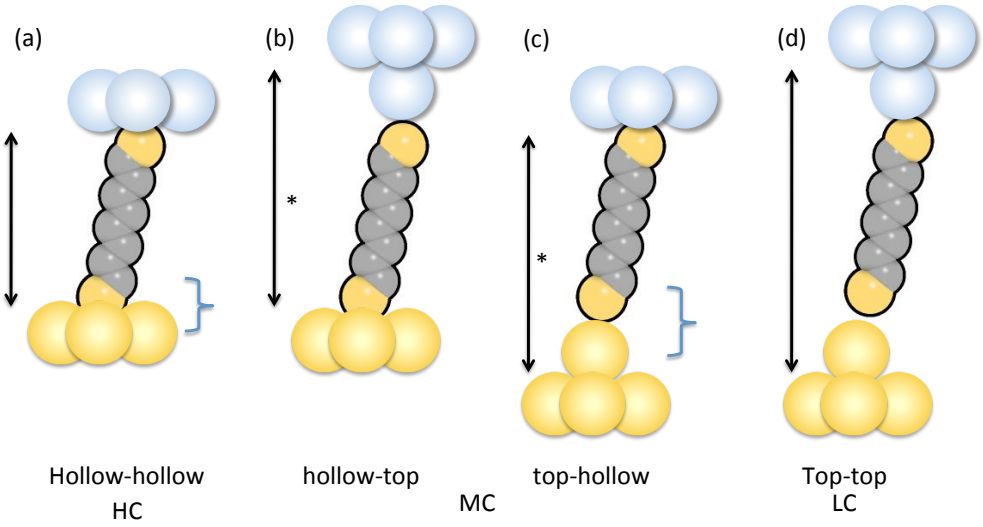

Figure 4.5: The proposed configurations for the metal-molecule-metal system. Hollow-hollow (HC) (a), top-hollow (MC) in (b),(c), and top-top (LC) (d). The distance between the thiol-ligand and a metal electrode, as well as the number of atoms which the thiol ligand binds to mostly decide a contact conductances of a ODT. The MC distances denoted (*) are identical when the metal electrodes both side are the same, and different when the metal on either side is different.

Strong binding creates lower contact resistance. For molecular contacts, thiols and phosphines (PMe_2) have strong binding energies and thus show higher conductance values, while carboxyl (COOH) and amine (NH_2) have relatively weak binding energies and thus show lower conductance values [72, 38].

Thus, the dependence of the conductance on the strength of chemical binding corroborates that stronger binding leads to the higher conductance value of a molecule bound to

the platinum electrode.

Both the chemical binding and the distance between a molecule and the electrode affect the conduction mechanism in this case where the current goes from one electrode to the other through the ODT. There apparently exist three kinds of binding configuration for these electrodes. I propose that the conductance value of the top-hollow configuration corresponds to MC (medium conductance). Similarly, I will associate LC with the peak found using the control experiments. The schematic binding geometries for HC, MC, and LC are indicated in Fig. 4.5.

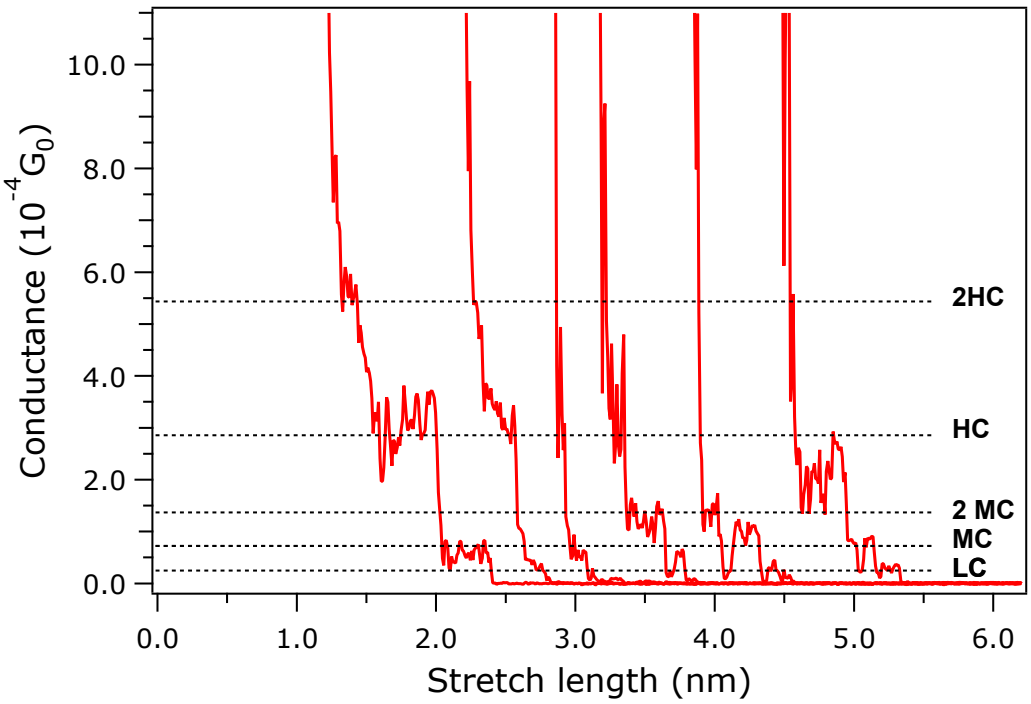

Figure 4.6: Pt-ODT-Au current-distance traces at 0.1 V, showing the HC, MC and LC series. Inset: zoom-in view of the same traces to show the LC and the MC more closely. The existence of LC steps were observed through current-distance traces. The LC conductance value is close to the baseline and can be more clearly distinguished on the logarithmic plot in Fig. 4.2.

The conductance value of LC is inferred to be $(0.24 \pm 0.07) \times 10^{-4}$ G_0 based on the histogram divided by that of the control experiment (Fig. 4.2 (b)). The observed MC value

is 0.65×10^{-4}, and the HC value is 2.8×10^{-4} G_0. The intermediate value of the MC conductance value suggests that it corresponds to a configuration where the hollow site on (Au) is connected to the top site on (Pt). We will discuss this idea further in the next section. The HC, MC, and LC series are observed in current-distance curves, as well (see Fig. 4.6). The location of each series also matches the peaks from the histogram analysis. Thus, as we can see from Fig. 4.2, using control experiments to reduce the background events, we can identify more clearly three series of peak locations, which we associate with three cases of binding.

The MC and HC configurations have been hypothesized to result from a sulfur atom at one side residing in the hollow site of the metal substrate. However, a recent study claims that bridge binding (where the sulphur atom binds to two gold atoms) is more stable than hollow binding (S binds to three Au atoms) [88, 89, 90]. But whether the hollow is actually bridge binding or not, there are definitely three possible configurations.

4.2 Measurement of Voltage-Dependent Properties at Thiol-Metal Junctions

Understanding charge transport mechanisms across single-molecule junctions is very important for possible applications of nanoscale device developments. The conductance measurements as a function of voltage can confirm the electronic properties at the junction as well as for a molecule. We carried out measurements of the conductance of each system (Au-ODT-Au, Pt-ODT-Au, and Pt-ODT-Pt) as a function of bias voltage (V_{bias}). The conduction mechanism for alkanedithiols is pure tunneling, with an exponential decay over a length β^{-1} (See Sect. 1.2). In the tunneling process, the current-voltage dependence of ODT (the current values of LC, MC, and HC) will linearly increase as the bias voltage increases, for small voltages (< 0.4 V). For example, for the Au-ODT-Au system, the location of LC and HC peaks were almost same, for bias voltages up to 0.4 V, as shown in Fig. 4.7 (a), and as also previously observed [59, 31, 83].

However, the overall conductance of metal-molecule-metal system depends greatly on the junction between the thiol ligand and the electrode. Since Pt and Au have different binding strengths, work functions, and electron states for conduction, the three systems

should show different conductances. In the first section, we describe the bias-dependent behavior of the conductance of Pt-ODT-Au system in detail.

In addition, the dependence of conductance on bias voltage also relates to the stability of the junction between a electrode and a ligand. We will investigate junction stability as a function of bias voltage in the second section.

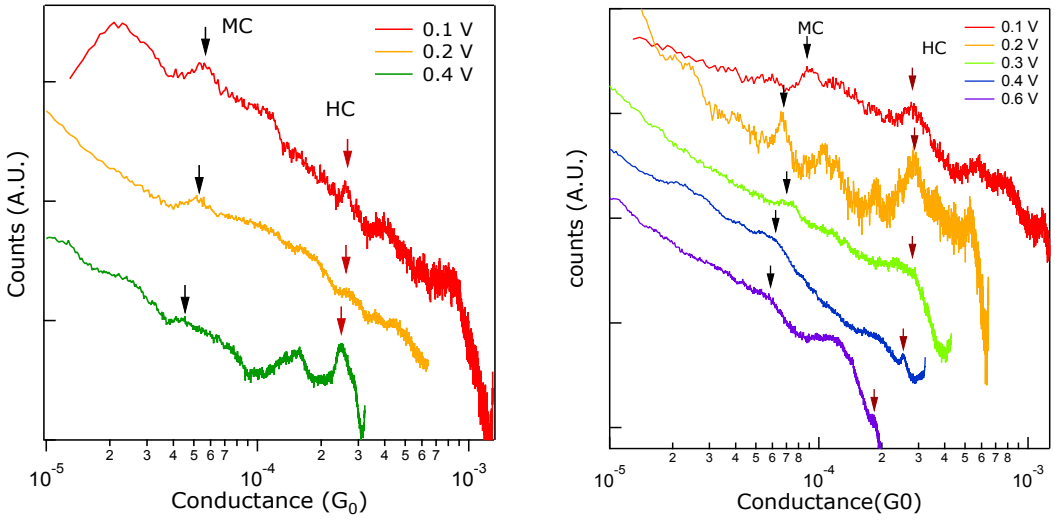

(a) Au-ODT-Au system

(b) Pt-ODT-Au system

Figure 4.7: Conductance histograms as a function of increasing bias voltage from Au-ODT-Au system (a), and Pt-ODT-Au system (b). Conductance of (a) is almost constant as bias voltage increases, while peaks in (b) decreased drastically from 0.4 V to 0.6 V. Spring constant was k = 1.4 – 1.6 nN/nm for gold and 30 – 50 nN/nm for platinum tips.

4.2.1 Nonlinear conductance of transition metal-molecule-metal system as a function of bias voltage

Figure 4.7 shows conductance histograms of the Au-ODT-Au and Pt-ODT-Au configurations as the bias voltage increases from 0.1 V to 0.6 V. The locations of the HC and MC peaks are shown in Fig. 4.8.

As the bias voltage was increased, the HC and MC conductances in both systems were

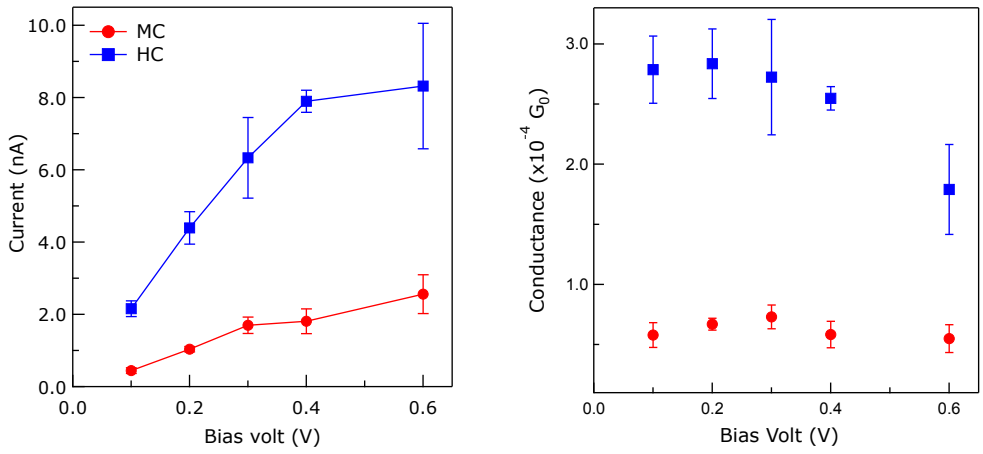

(a) (b)

Figure 4.8: Bias-dependent conductance for Pt-ODT-Au system as measured by (a) current, (b) conductance (G_0). Error bars represent the conductance peak width as determined by a Gaussian curve fit.

almost the same but tended to smoothly decrease as the bias voltage was increased. The MC conductance did not change appreciably (0.7 to 0.53 $\times 10^{-4}$ G_0), while the HC conductance of Pt-ODT-Au reduced drastically over 0.4 V, as shown in Fig. 4.8. For the case of 0.6 V, I found a peak at 1.79×10^{-4} G_0, almost half from the value at 0.1 V. To confirm the peak location, I compiled conductance histograms using the low-gain amplifier (1 μA/V) over a range of bias voltages from 0.2 to 0.6 V. The low-gain amplifier simultaneously measures current with the high-gain amplifier (1 nA/V) in the dual-gain cantilever holder (See Sect. 3.1). The locations of the two histograms were shifted because of a systematic offset of the dual-gain amplifier (1.4 $\times 10^{-8}$ A offset). However, they showed same trend as those of high-gain amplifier. The HC conductance at 0.1 V could not be acquired using the low-gain amplifier because we were not able to resolve any peaks over the higher background noise of the low-gain amplifier (1 to 2 nA).

Dalgleish *et al.* calculated for a thiol-metal interface that hybridization between molecular thiol and surface states of transition metal contacts will form metal-induced gap states called "interface states." For Pd and Pt, the interface states will form near the Fermi energy.

The resonance of the interface states of the junction and chemical potentials at each side can give rise to a decrease in current as the bias voltage increase, a phenomenon known as negative differential resistance (NDR) [40, 91]. Negative differential resistance is well-known in semiconductor physics, for example in the Esaki tunneling diode [92]. We hypothesize that the nonlinearity of the I–V characteristic of the Pt-ODT-Au system results from interaction of the resonance of interface states at the Pt-thiol junction with the Fermi level of the other electrode as the bias voltage is increased.

Dalgleish *et al.* claimed, based on their calculations, that the resonance of interface states for the source electrode contributes to nonlinearity that can result in NDR for the metal-molecule-metal system with transition metal electrodes, such as a Pt-ODT-Pt system [91]. The same theory can also be applied to the Pt-ODT-Au system. At zero forward bias voltage [Au (+) and Pt (-)], the interface state forms near the Fermi energy of the Pt electrode and has a distribution along the state as in Fig. 4.9 (a). Since the interface state in Au is known to play only a minimal role in charge transport mechanism through the MMM system, only the interface states at Pt side will be considered.

As the bias voltage is increased, the potential energy of electron at the Au junction decreases, and the electron energy at the Pt junction increases. Then, the energy envelope of the interface states at Pt electrode also increases and starts entering the window, and the Fermi energy level at Au junction becomes lower. While the "window" between E_F of Pt and Au is within the interface resonance of the Pt electrode, the current increases as the bias voltage increases and reaches maximum near V_{bias} = 0.4 V as in Fig. 4.9 (b). As the bias voltage increases further until the distribution of the interface states completely entered the window as in Fig. 4.9 (c), the current saturates even at increasing bias voltage. We did not observe NDR in this system, but the nonlinear I–V may still result from an influence from the resonance of the interface states in the Pt electrode.

According to the calculation of Dalgleish *et al.*, the interface state forms in the Pt electrode when the thiol ligand is in a hexagonal close-packed (HCP) configuration, that is in the HC configuration. Since the interface state forms in the Pt electrodes, the effect from the interface states should be significant when the ligand is physically close to the metal electrode. Therefore, in the MC and LC configurations, the nonlinearity did not appear. In the MC configuration, there should be two possibilities as depicted in (b) and (c) of Fig. 4.5. One is an ODT connecting the hollow site of Au with the top site of Pt, and vice

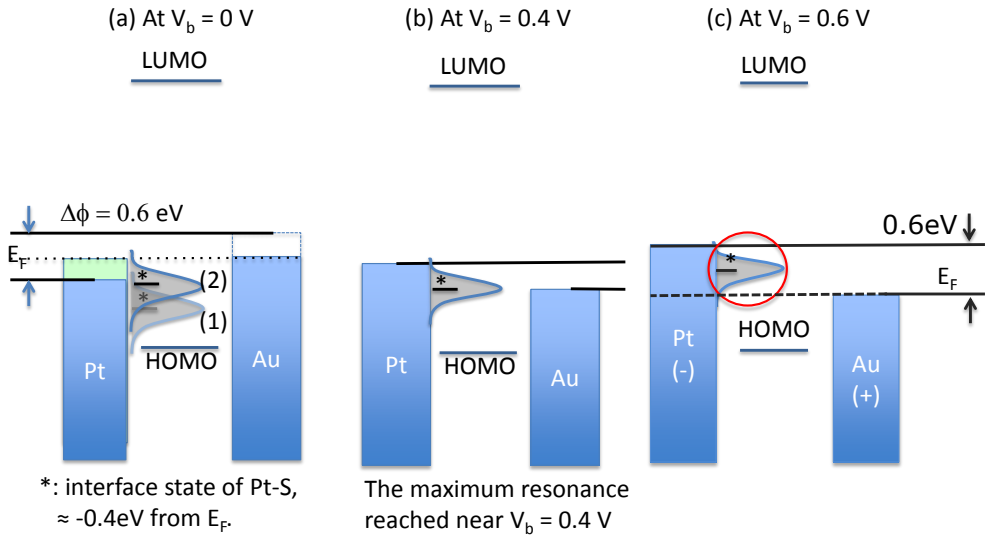

Figure 4.9: Diagram for the energy-level alignment of the Pt-ODT-Au system. $\Delta\phi$ is the difference between work functions at the Au and Pt electrodes, and (*) denotes the interface state distribution of Pt hybridized with thiol ligand. (a) At zero bias voltage, interface states form in a Pt electrode near Fermi level ($\approx$ 0.4 eV below the Fermi level). Because of an intrinsic difference between the work functions of Au and Pt, the level moves until it reaches the same E_F [(1): before the Pt-ODT-Au configuration is made, (2): after connection is made between the Pt and Au electrodes.] As the bias voltage is increased, the current increases. As the envelope of the resonance enters the window between the Fermi level of Pt and Au, transmission is enhanced and rises to a maximum at near V_{bias} = 0.4 V, as in (b). Once the resonant peak of interface states of Pt electrode passes E_F, the current saturates and does not increase much as the bias voltage increases (c).

versa. Since the conductance value did not change as the bias voltage was increased, the configuration is likely to be one where the ODT connects the hollow site of Au with the top site of Pt atoms. This hypothesis seems reasonable because we carried out break-junction measurements on ODT SAMs on gold surfaces. For stable SAMs, a thiol ligand connects three Au atoms as we discussed in Sect. 1.1.

4.2.2 Stability of single-molecular junctions evaluated by measuring conductance plateau lengths

In Sec. 4.1, we discussed how the binding strength and the number of transport channels determine the conductance of the Pt-ODT-Au, and the Au-ODT-Au system. In Sec. 4.2.1, we observed a decrease of conductance with bias voltage and attributed the observation to a resonance of the interface states. In this section, we investigated how the strength of the bonding relates to the bias voltage to find out whether this resonance affects the strength of a thiol-platinum bond.

To evaluate the bond strength, we measured the stretch length at the conductance value [HC and MC (previously LC)] of each current trace. Evans *et al.* developed a theory to explain the effect of chemical bonding under an external force, as depicted in Fig. 4.10 [93, 94]. Since bond breaking is associated with the force to escape from a potential well, an external force is applied, the barrier E_b is rotated and lowered, decreasing the escape time to

$$\tau = \tau_0 \cdot \exp[\frac{E_b(f)}{k_B T}], \tag{4.1}$$

where $E_b(f)$ is the barrier height for an applied force and $k_b T$ is the thermal energy.

Since the lifetime of the bond depends on its environment, binding strength and temperature [94], we can use stretch lengths of the HC and MC values as a method to measure the bond strength at a given temperature [60, 69, 54].

Huang *et al.* used the stretch length of the MC conductance step to measure a local temperature at a junction between Au and thiol ligand. They observed a shortening of the length as the bias voltage increased, using STMBJ [69], and using C-AFM, they observed the force needed to rupture the bond showed the same trends as the bias voltage increased [60]. They interpreted this phenomenon as the local temperature at the Au-S junction, which increases as the V_{bias} increases.

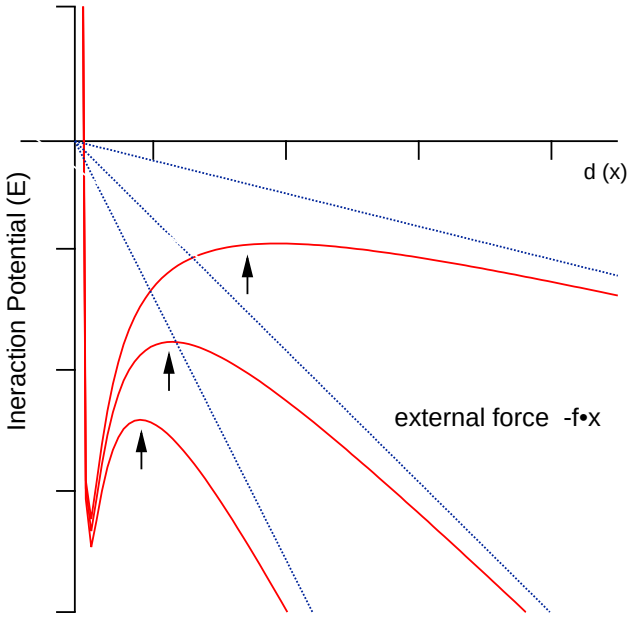

Figure 4.10: Potential landscape for chemical bonding. The energy landscape is rotated (by $-f \cdot x$) as an external force is applied. As a consequence, the energy barrier is lowered until the binding with binding energy E_b breaks. As the pulling force is increased, the energy barrier is reduced in height and also narrows.

The way we measured stretch lengths of each current-distance curve is described in Sect. 3.2.2. We measured the stretch length for traces of each bias voltage and showed the average stretch lengths of them in Fig. 4.11. Since the stiffness of AFM cantilevers affects the stretch lengths, all the cantilevers used here are from the same manufacturer and have the same nominal stiffness (k = 30–50 nN/nm). The measurements for 0.3, 0.4, and 0.6 V all used a single cantilever.

As we can see from Fig. 4.11, the length of the HC peak sharply decreases for V_{bias} > 0.4 V, whereas MC lengths decreased only gradually. We observed the average stretch length is even less at V_{bias} = 0.4 V than the length at 0.6 V. If we combine this result with the result in previous section, we can relate this to the fact that the resonance peak of the interface states at the Pt electrode is about 0.4 eV less than the Fermi level.

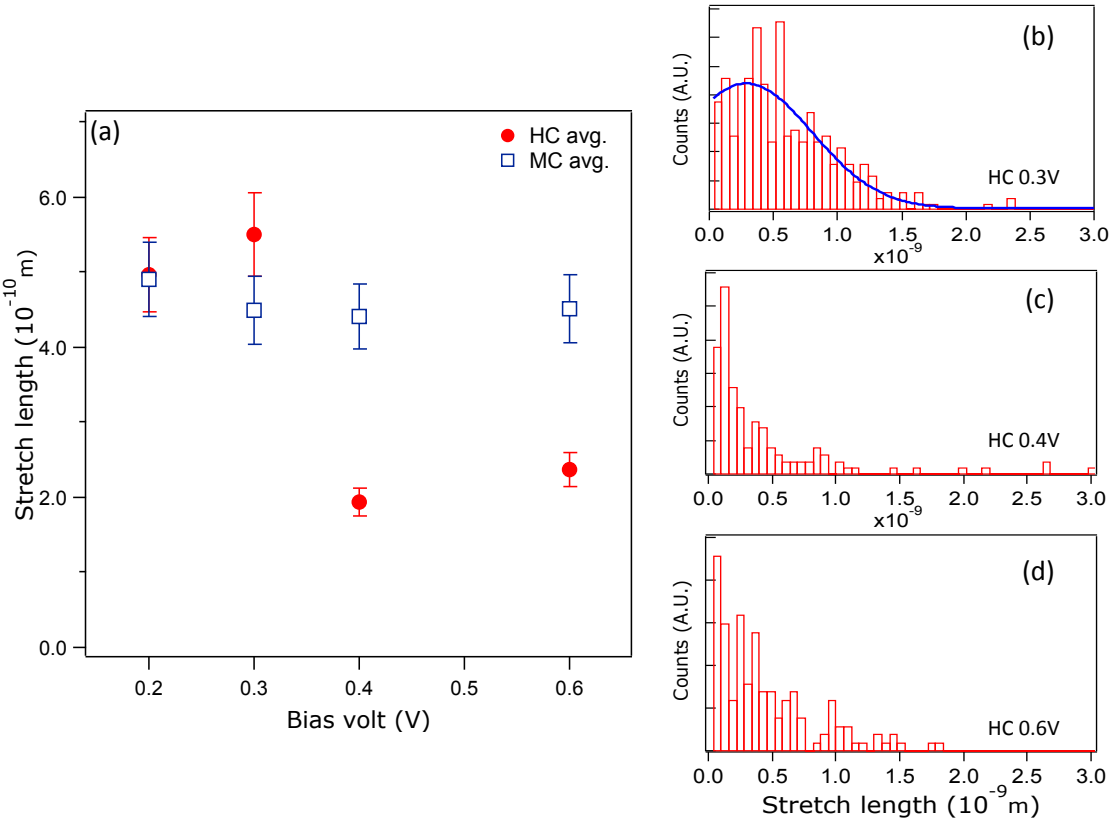

Figure 4.11: The average values of stretch lengths measured from current-distance traces, for different bias voltages. While the MC average decreases relatively gradually, the HC lengths sharply decrease above 0.4 V bias. (b),(c),(d) are histograms of the stretch lengths compiled at V_b = 0.3, 0.4, and 0.6 V. As the bias voltage increases, spontaneous breaking increases.

Therefore, we can hypothesize that the resonance weakens the binding between the ODT thiol group and the Pt electrode. In other words, the resonance peak raises the local temperature at the Pt-thiol junction, which shortens the average stretch length of the junction at 0.4 V.

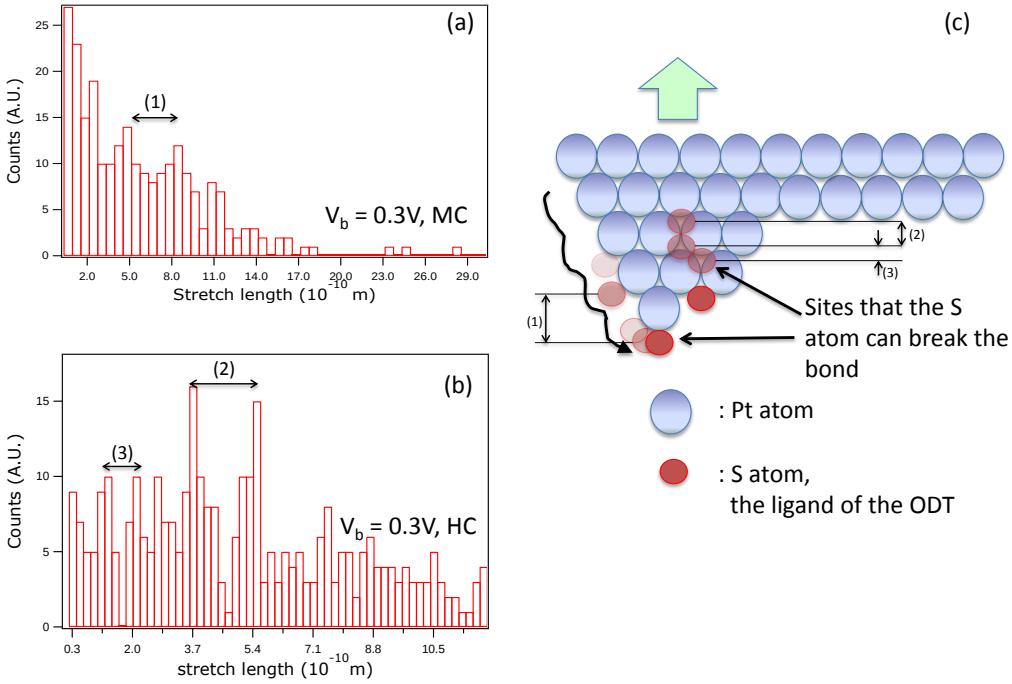

Figure 4.12: A stretch length histogram shows a lattice-matching periodicity. An ODT molecule can be pulled and slide along the Pt atoms on AFM tip as the cantilever is pulled away from the substrate. (a) The stretch length histogram show a periodicity of about 3 Å (see (1) on figure) for the MC case. (b) For the HC case, the stretch-length oscillations can be 1.7 Å (see (2) on figure) or 0.9 Å (see (3) on figure). (c) Diagram showing possible mechanisms at the tip. Since we assume a dense ODT SAMs, this phenomenon is more likely to occur on the tip surface than on the substrate.

While analyzing the stretch-length histograms, we observed a small, but interesting feature: A periodicity in counts in the stretch-length histogram. As we can see in Fig. 4.12, a ripple in the MC peak started near 2 Å and repeated at roughly 3 Å intervals.

The periodicity coincides with the diameter of gold and platinum, ($\approx$ 3 Å). For the HC configuration, we observed a $\approx$ 1.7 Å periodicity. The oscillations in the HC case were weaker than the MC case. Based on these observations, I can hypothesize that the ODT bond rupture occurs in two stages: first, the molecule is pulled from its initial site but remains non-specifically bound (either to the substrate or the tip, as the case may be). Then the molecule is dragged a short distance along the surface until it finally ruptures completely. The oscillations in the histogram then reflect a tendency to stay longer in places where further bonds can form.

For the MC case, a thiol ligand can slide from the top of one electrode atom to another, until it unbinds. For the HC case, since the configuration forms where the ligand binds to three Au or Pt atoms at the center of the respective face-centered cubic (fcc) or hcp structure, the stretch length for HC increases with a periodicity that matches the distance from the fcc configuration to the hcp configuration. When the HC configuration is broken, the atom can either rupture three bonds to be out of the junction or rupture one or two bonds and slide to the top of one electrode atom and can thereby turn into an MC configuration.

Another possibility is that a gold atom attached to a thiol bond can slide along the substrate. Such a sliding motion could also have a 3 Å periodicity. To confirm the configuration and origin of the histogram oscillations, one would need to do a further study of the electrical and mechanical properties of the thiol-Au and thiol-Pt configurations.

To address these hypotheses, we could, in principle, analyze the phonon interaction at given bias voltages using inelastic electron transport spectroscopy (IETS) analysis for the junction. Such experiments would be beyond the scope of this thesis, and we leave this question for future work.

Chapter 5

Conclusion

In this thesis, we used the simplest molecule 1,8-octanedithiol (ODT) to explore the charge transport mechanisms at the junction between thiol and metal electrode. We presented two investigations of the conduction mechanism in metal-molecule-metal systems.

First, we used the break-junction technique to argue that the conductance of ODT depends on the geometric configuration (the distance between electrode and ligand), the binding strength, and the number of electron transport channels in different metal-molecule-metal systems (Au-ODT-Au, Pt-ODT-Au, and Pt-ODT-Pt). The difference between electronic states of Au and Pt electrodes and the number of bonds that a thiol ligand can make affects the number of channels available for electron transport. The strong binding between thiol and metal electrodes draws the two objects closer to each other and increases charge transport.

Second, we investigated the influence of bias voltage on conductance. We observed a sharp decrease of conductance at 0.6 V. We attribute this to an alignment of interface states within the junction, as suggested by a theory of Dalgleishi *et al.* The interpretation is supported qualitatively by the data. We also observed that the stretch length at 0.4V decreases abruptly for HC bonds. We hypothesize that the resonance of interface states at the junction could raise the local temperature at the junction. Both the conductance and stretch length affect only HC-bonded molecules, where thiol binds to three platinum atoms.

Although the results presented here make sense physically and are qualitatively consistent with expectations, a more detailed theoretical investigation is needed to confirm my interpretations. A simulation of the theoretical model would help understand better the

experimental results and could clarify the charge-transport mechanism through metal-thiol junctions. If a simulation for structural difference is carried out based on this work and if the distances between sulfur-Au or sulfur-Pt in each configuration can be calculated, one should be able to understand and predict different conductance values of alkanes connected to various metal electrodes.

In addition, experiments on the electrical properties of reverse-biased Pt- ODT-Au and Pt-ODT-Pt would be an interesting complement to the studies begun here.

Consequently, here we have added one more work on the charge transport mechanism for metal-molecule-metal systems. We showed that it is possible to manipulate electronic properties of simple metal-molecule-metal systems just by using different metal electrodes. We hope that this work will lead to a better understanding of the charge transport mechanisms between molecular ligands and metal electrodes.

Bibliography

[1] Carroll, R. L. & Gorman, C. B. The genesis of molecular electronics. *Angew. Chem. Int. Ed. Engl.* **41**, 4378–4400 (2002).

[2] Feynman, R. P. Plenty of room at the bottom. In *Presentation to the American Physical Society* (1959).

[3] Lu, S. *Conductivity measurements of single DNA molecules using conductive-atomic force microscopy*. M.Sc. thesis, Simon Fraser University (2006).

[4] Aviram, A. & Ratner, M. A. Molecular rectifiers. *Chem. Phys. Lett.* **29**, 277–283 (1974).

[5] Nitzan, A. & Ratner, M. A. Electron transport in molecular wire junctions. *Science* **300**, 1384–1389 (2003).

[6] Tao, N. J. Electron transport in molecular junctions. *Nature Nanotech.* **1**, 173–181 (2006).

[7] Dalgleish, H. *Electron Transport in Molecular Wires with Transition Metal Contacts*. Ph.D. thesis, Simon Fraser University (2006).

[8] Reed, M. A., Zhou, C., Muller, C. J., Burgin, T. P. & Tour, J. M. Conductance of a molecular junction. *Science* **278**, 252–254 (1997).

[9] Datta, S. *et al.* Current-voltage characteristics of self-assembled monolayers by scanning tunneling microscopy. *Phys. Rev. Lett.* **79**, 2530–2533 (1997).

[10] Love, J. C., Estroff, L. A., Kriebel, J. K., Nuzzo, R. G. & Whitesides, G. M. Self-assembled monolayers of thiolates on metals as a form of nanotechnology. *Chem. Rev.* **105**, 1103–1169 (2005).

[11] Ulman, A. Formation and structure of self-assembled monolayers. *Chem. Rev.* **96**, 1533–1554 (1996).

[12] Tao, F. & Bernasek, S. L. Understanding odd-even effects in organic self-assembled monolayers. *Chem. Rev.* **107**, 1408–1453 (2007).

[13] Bezryadin, A., Dekker, C. & Schmid, G. Electrostatic trapping of single conducting nanoparticles between nanoelectrodes. *Appl. Phys. Lett.* **71**, 1273–1275 (1997).

[14] Park, H., Lim, A., Alivisatos, A., Park, J. & McEuen, P. Fabrication of metallic electrodes with nanometer separation by electromigration. *Appl. Phys. Lett.* **75**, 301 (1999).

[15] Binnig, G., Rohrer, H., Gerber, C. & Weibel, E. Surface studies by scanning tunneling microscopy. *Phys. Rev. Lett.* **49**, 57–61 (1982).

[16] Binnig, G., Quate, C. F. & Gerber, C. Atomic force microscope. *Phys. Rev. Lett.* **56**, 930–933 (1986).

[17] Maksymovych, P., Voznyy, O., Dougherty, D., Sorescu, D. & Jr, J. Y. Gold adatom as a key structural component in self-assembled monolayers of organosulfur molecules on Au (111). *Prog. in Surf. Sci.* **85**, 206–240 (2010).

[18] Jadzinsky, P. D., Calero, G., Ackerson, C. J., Bushnell, D. A. & Kornberg, R. D. Structure of a thiol monolayer-protected gold nanoparticle at 1.1 Å resolution. *Science* **318**, 430–433 (2007).

[19] Frasconi, M., Mazzei, F. & Ferri, T. Protein immobilization at gold-thiol surfaces and potential for biosensing. *Anal. Bioanal. Chem.* **398**, 1545–1564 (2010).

[20] Shan, X., Patel, U., Wang, S., Iglesias, R. & Tao, N. Imaging local electrochemical current via surface plasmon resonance. *Science* **327**, 1363–1366 (2010).

[21] Wang, W., Lee, T. & Reed, M. Mechanism of electron conduction in self-assembled alkanethiol monolayer devices. *Phys. Rev. B* **68**, 35416 (2003).

[22] Cui, X. *et al.* Reproducible measurement of single-molecule conductivity. *Science* **294**, 571–574 (2001).

[23] Holmlin, R. E. *et al.* Electron transport through thin organic films in metal-insulator-metal junctions based on self-assembled monolayers. *J. Am. Chem. Soc.* **123**, 5075–5085 (2001).

[24] Chabinyc, M. L. *et al.* Molecular rectification in a metal-insulator-metal junction based on self-assembled monolayers. *J. Am. Chem. Soc.* **124**, 11730–11736 (2002).

[25] Bumm, L., Arnold, J., Dunbar, T. & Allara, D. Electron transfer through organic molecules. *J. Phys. Chem.* **103**, 8122–8127 (1999).

[26] Wold, D. & Frisbie, C. Fabrication and characterization of metal-molecule-metal junctions by conducting probe atomic force microscopy. *J. Am. Chem. Soc.* **123**, 5549–5556 (2001).

[27] Engelkes, V. B., Beebe, J. M. & Frisbie, C. D. Length-dependent transport in molecular junctions based on sams of alkanethiols and alkanedithiols: Effect of metal work function and applied bias on tunneling efficiency and contact resistance. *J. Am. Chem. Soc.* **126**, 14287–14296 (2004).

[28] Choi, S. H., Kim, B. & Frisbie, C. D. Electrical resistance of long conjugated molecular wires. *Science* **320**, 1482–6 (2008).

[29] Choi, S. H. *et al.* Transition from tunneling to hopping transport in long, conjugated oligo-imine wires connected to metals. *J. Am. Chem. Soc.* **132**, 4358–4368 (2010).

[30] Kelley, S., Jackson, N., Hill, M. & Barton, J. Long-range electron transfer through DNA films. *Angew. Chem. Int. Ed. Engl.* **38**, 941–945 (1999).

[31] Li, X., Tao, N. & Lindsay, S. Conductance of single alkanedithiols: Conduction mechanism and effect of molecule-electrode contacts. *J. Am. Chem. Soc.* **128**, 2135–2141 (2006).

[32] Salomon, A. *et al.* Comparison of electronic transport measurements on organic molecules. *Adv. Mater.* **15**, 1881–1890 (2003).

[33] Chen, F., Hihath, J., Huang, Z., Li, X. & Tao, N. Measurement of single-molecule conductance. *Ann. Rev. Phys. Chem.* **58**, 535–564 (2007).

[34] Haiss, W. *et al.* Impact of junction formation method and surface roughness on single molecule conductance. *J. Phys. Chem. C* **113**, 5823–5833 (2009).

[35] Kirczenow, G. *Molecular nanowires and their properties as electrical conductors*, vol. 1 of *The Oxford Handbook of Nanoscience and Technology* (Oxford University Press, 2010).

[36] Emberly, E. G. & Kirczenow, G. Theoretical study of electrical conduction through a molecule connected to metallic nanocontacts. *Phys. Rev. B* **58**, 4–8 (1998).

[37] Venkataraman, L. *et al.* Single-molecule circuits with well-defined molecular conductance. *Nano Lett.* **6**, 458–462 (2006).

[38] Chen, F., Li, X., Hihath, J., Huang, Z. & Tao, N. Effect of anchoring groups on single-molecule conductance: Comparative study of thiol-, amine-, and carboxylic-acid-terminated molecules. *J. Am. Chem. Soc.* **128**, 15874–15881 (2006).

[39] Engelkes, V. B., Beebe, J. M. & Frisbie, C. D. Analysis of the causes of variance in resistance measurements on metal-molecule-metal junctions formed by conducting-probe atomic force microscopy. *J. Phys. Chem. B* **109**, 16801–16810 (2005).

[40] Dalgleish, H. & Kirczenow, G. Interface states, negative differential resistance, and rectification in molecular junctions with transition-metal contacts. *Phys. Rev. B* **73**, 245431 (2006).

[41] Binnig, G. & Rohrer, H. Scanning tunneling microscopy—from birth to adolescence. *Rev. Mod. Phys.* **59**, 615–625 (1987).

[42] Beebe, J. M., Kim, B., Gadzuk, J. W., Frisbie, C. D. & Kushmerick, J. G. Transition from direct tunneling to field emission in metal-molecule-metal junctions. *Phys. Rev. Lett.* **97**, 026801 (2006).

[43] Reichert, J. *et al.* Driving current through single organic molecules. *Phys. Rev. Lett.* **88**, 176804 (2002).

[44] Cui, X. *et al.* Making electrical contacts to molecular monolayers. *Nanotechnology* **13**, 5–14 (2002).

[45] Ouisse, T. *Electron Transport in Nanostructures and Mesoscopic Devices: An introduction* (ISTE and John Wiley & Sons, Inc., 2008).

[46] Morita, T. & Lindsay, S. Determination of single molecule conductances of alkanedithiols by conducting-atomic force microscopy with large gold nanoparticles. *J. Am. Chem. Soc.* **129**, 7262–7263 (2007).

[47] Chao, W., Harteneck, B., Liddle, J. & Anderson, E. Soft X-ray microscopy at a spatial resolution better than 15 nm. *Nature* **435**, 1210–1213 (2005).

[48] Park, H., Park, J., Lim, A., Anderson, E. & Alivisatos, A. Nanomechanical oscillations in a Single-C_{60} transistor. *Nature* **407**, 57–60 (2000).

[49] Liang, W., Shores, M. P., Bockrath, M., Long, J. R. & Park, H. Kondo resonance in a single-molecule transistor. *Nature* **417**, 725–729 (2002).

[50] Song, H. *et al.* Observation of molecular orbital gating. *Nature* **462**, 1039–1043 (2009).

[51] Trouwborst, M. L., Huisman, E. H., Bakker, F. L., van der Molen, S. J. & van Wees, B. J. Single atom adhesion in optimized gold nanojunctions. *Phys. Rev. Lett.* **100**, 175502 (2008).

[52] Scheer, E., Joyez, P., Esteve, D. & Urbina, C. Conduction channel transmissions of atomic-size aluminum contacts. *Phys. Rev. Lett.* **78**, 3535–3538 (1997).

[53] Huisman, E. H. *et al.* Stabilizing single atom contacts by molecular bridge formation. *Nano Lett.* **8**, 3381–3385 (2008).

[54] Tsutsui, M., Shoji, K., Morimoto, K., Taniguchi, M. & Kawai, T. Thermodynamic stability of single molecule junctions. *Appl. Phys. Lett.* **92**, 223110 (2008).

[55] Horiguchi, K., Tsutsui, M., Kurokawa, S. & Sakai, A. Electron transmission characteristics of Au/1,4-benzenedithiol/Au junctions. *Nanotechnology* **20**, 025204 (2009).

[56] Tsutsui, M., Taniguchi, M. & Kawai, T. Atomistic mechanics and formation mechanism of metal-molecule-metal junctions. *Nano Lett.* **9**, 2433–2439 (2009).

[57] Xu, B. & Tao, N. J. Measurement of single-molecule resistance by repeated formation of molecular junctions. *Science* **301**, 1221 (2003).

[58] Xiao, X., Xu, B. & Tao, N. J. Measurement of single molecule conductance: Benzenedithiol and benzenedimethanethiol. *Nano Lett.* **4**, 267 (2004).

[59] Xu, B., Xiao, X. & Tao, N. J. Measurements of single-molecule electromechanical properties. *J. Am. Chem. Soc.* **125**, 16164–16165 (2003).

[60] Huang, Z., Xu, B., Chen, Y., Ventra, M. D. & Tao, N. Measurement of current-induced local heating in a single molecule junction. *Nano Lett.* **6**, 1240–1244 (2006).

[61] Fujihira, M., Suzuki, M., Fujii, S. & Nishikawa, A. Currents through single molecular junction of Au/hexanedithiolate/Au measured by repeated formation of break junction in STM under UHV: Effects of conformational change in an alkylene chain from gauche to trans and binding sites of thiolates on gold. *Phys. Chem. Chem. Phys.* **8**, 3876–3884 (2006).

[62] Nishikawa, A. *et al.* Accurate determination of multiple sets of single molecular conductance of Au/ 1,6-hexanedithiol/ Au break junctions by ultra-high vacuum-scanning tunneling microscope and analyses of individual current–separation curves. *Phys. Chem. Chem. Phys.* **18**, 424005 (2007).

[63] Haiss, W. *et al.* Redox state dependence of single molecule conductivity. *J. Am. Chem. Soc.* **125**, 15294–15295 (2003).

[64] Nichols, R. *et al.* The experimental determination of the conductance of single molecules. *Phys. Chem. Chem. Phys.* **12**, 2801–2815 (2010).

[65] Haiss, W. *et al.* Measurement of single molecule conductivity using the spontaneous formation of molecular wires. *Phys. Chem. Chem. Phys.* **6**, 4330–4337 (2004).

[66] Li, C. *et al.* Charge transport in single Au / alkanedithiol / Au junctions: coordination geometries and conformational degrees of freedom. *J. Am. Chem. Soc.* **130**, 318–326 (2008).

[67] Ko, C.-H., Huang, M.-J., Fu, M.-D. & Chen, C.-H. Superior contact for single-molecule conductance: Electronic coupling of thiolate and isothiocyanate on Pt, Pd, and Au. *J. Am. Chem. Soc.* **132**, 756–764 (2010).

[68] Xu, B. Q., Li, X. L., Xiao, X. Y., Sakaguchi, H. & Tao, N. J. Electromechanical and conductance switching properties of single oligothiophene molecules. *Nano Lett.* **5**, 1491–1495 (2005).

[69] Huang, Z. *et al.* Local ionic and electron heating in single-molecule junctions. *Nature Nanotech.* **2**, 698–703 (2007).

[70] Kamenetska, M. *et al.* Formation and evolution of single-molecule junctions. *Phys. Rev. Lett.* **102**, 126803 (2009).

[71] Beebe, J. M., Kim, B., Frisbie, C. D. & Kushmerick, J. G. Measuring relative barrier heights in molecular electronic junctions with transition voltage spectroscopy. *ACS Nano* **2**, 827–832 (2008).

[72] Park, Y. S. *et al.* Contact chemistry and single-molecule conductance: A comparison of phosphines, methyl sulfides, and amines. *J. Am. Chem. Soc.* **129**, 15768 (2007).

[73] Ko, C.-H., Huang, M.-J., Fu, M.-D. & Chen, C.-H. Superior contact for single-molecule conductance: electronic coupling of thiolate and isothiocyanate on Pt, Pd, and Au. *J. Am. Chem. Soc.* **132**, 756–764 (2010).

[74] Ulrich, J. *et al.* Variability of conductance in molecular junctions. *J. Phys. Chem. B* **110**, 2462–2466 (2006).

[75] Hihath, J., Bruot, C. & Tao, N. Electron-phonon interactions in single octanedithiol molecular junctions. *ACS Nano* **4**, 3823–3830 (2010).

[76] Csonka, S., Halbritter, A., Mihaly, G. & Jurdik..., E. Fractional conductance in hydrogen-embedded gold nanowires. *Phys. Rev. Lett.* **90**, 116803 (2003).

[77] Slowinski, K., II, R. C., Bilewicz, R. & Majda, M. Evidence for inefficient chain-to-chain coupling in electron tunneling through liquid alkanethiol monolayer films on mercury. *J. Am. Chem. Soc.* **118**, 4709–4710 (1996).

[78] Slowinski, K., Chamberlain, R., Miller, C. & Majda, M. Through-bond and chain-to-chain coupling. two pathways in electron tunneling through liquid alkanethiol monolayers on mercury electrodes. *J. Am. Chem. Soc.* **119**, 11910–11919 (1997).

[79] Song, H., Lee, H. & Lee, T. Intermolecular chain-to-chain tunneling in metal-alkanethiol-metal junctions. *J. Am. Chem. Soc.* **129**, 3806–3807 (2007).

[80] Qi, Y. *et al.* Mechanical and charge transport properties of alkanethiol self-assembled monolayers on a Au(111) surface: The role of molecular tiltolayers on a Au(111) surface: The role of molecular tilt. *Langmuir* **24**, 2219–2223 (2008).

[81] Park, J. Y., Qi, Y., Ashby, P. D., Hendriksen, B. L. M. & Salmeron, M. Electrical transport and mechanical properties of alkylsilane self-assembled monolayers on silicon surfaces probed by atomic force microscopy. *J. Chem. Phys.* **130**, 114705 (2009).

[82] Chen, F., Li, X., Hihath, J., Huang, Z. & Tao, N. Effect of anchoring groups on single-molecule conductance: Comparative study of thiol-, amine-, and carboxylic-acid-terminated molecules. *J. Colloid Interface Sci.* **73**, 045403 (2006).

[83] Widawsky, J. R. *et al.* Measurement of voltage-dependent electronic transport across amine-linked single-molecular-wire junctions. *Nanotechnology* **20**, 434009 (2009).

[84] Haiss, W. *et al.* Anomalous length and voltage dependence of single molecule conductance. *Phys. Chem. Chem. Phys.* **11**, 10831–10838 (2009).

[85] Seminario, J., Cruz, C. D. L. & Derosa, P. A theoretical analysis of metal-molecule contacts. *J. Am. Chem. Soc* **123**, 5616–5617 (2001).

[86] Laiho, T. *et al.* Chemisorption of alkyl thiols and S-alkyl thiosulfates on Pt(111) and polycrystalline platinum surfaces. *Surf. Sci.* **584**, 83–89 (2005).

[87] Illas, F., Ricart, J. M. & Clotet, A. Bonding of atomic S to Pt(111) from ab initio explicitly correlated cluster model wave functions. *J. Phys. Chem. A* **101**, 9732–9737 (1997).

[88] Hu, Y., Zhu, Y., Gao, H. & Guo, H. Conductance of an ensemble of molecular wires: a statistical analysis. *Phys. Rev. Lett.* **95**, 156803 (2005).

[89] Cossaro, A. *et al.* X-ray diffraction and computation yield the structure of alkanethiols on gold(111). *Science* **321**, 943–6 (2008).

[90] Demir, F. & Kirczenow, G. Communication: Identification of the molecule-metal bonding geometries of molecular nanowires. *J. Chem. Phys.* **134**, 121103 (2011).

[91] Dalgleish, H. & Kirczenow, G. A new approach to the realization and control of negative differential resistance in single-molecule nanoelectronic devices: Designer transition metal-thiol interface states. *Nano. Lett.* **6**, 1274–1278 (2006).

[92] Esaki, L. New phenomenon in narrow germanium *p-n* junctions. *Phys. Rev.* **109**, 603–604 (1958).

[93] Evans, E. & Ritchie, K. Dynamic strength of molecular adhesion bonds. *Biophys. J.* **72**, 1541–1555 (1997).

[94] Evans, E. Probing the relation between force life time and chemistry in single molecular bonds. *Ann. Rev. Biophys. Biomol. Struct.* **30**, 105–128 (2001).